Editor's Note: *This is the eighty-fifth in a series of review and tutorial papers on various aspects of acoustics.*

On the oscillations of musical instruments

M. E. McIntyre
Department of Applied Mathematics and Theoretical Physics, University of Cambridge, Cambridge, CB3 9EW, England

R. T. Schumacher
Department of Physics, Carnegie-Mellon University, Pittsburgh, Pennsylvania 15213

J. Woodhouse
Topexpress Ltd., 1 Portugal Place, Cambridge, CB5 8AF, England

(Received 20 August 1982; accepted for publication 28 July 1983)

The time-domain description of musical and other nonlinear oscillators complements the more commonly used frequency-domain description, and is advantageous for some purposes. It is especially advantageous when studying large-amplitude oscillations, for which nonlinearity may be severe. It gives direct insight into the physical reasons for the variation of waveform as playing conditions vary, and into certain phenomena which may seem counter-intuitive from the frequency-domain viewpoint, such as the musically undesirable flattening in the pitch of a bowed string when the bow is pressed too hard onto the string. It is easy to set up efficient time-domain simulations on a small computer, a fact that has been surprisingly little exploited in musical acoustics. The simplest relevant model is described here. It demonstrates some of the basic nonlinear behavior of the clarinet, violin, and flute families with very little programming effort. Remarkably, a single set of model equations has relevance to all three cases, at a certain level of idealization, with appropriate choices of parameter values and of linear and nonlinear characteristics. For the flute family, this simplest model gives waveforms and phase relations closely resembling those observed at resonance in the organ-pipe experiments of Coltman [J. Acoust. Soc. Am. **60**, 725–733 (1976)], including the triangular pressure and velocity waveforms. It can be shown (again using a time-domain approach) that the triangular waveform is a universal limiting form, independent of detailed acoustic loss mechanisms provided losses are small.

PACS numbers: 43.10.Ln, 43.75. – z, 43.40.At

INTRODUCTION

It is an almost instinctive reaction among physicists to describe vibrating mechanical systems in terms of their normal modes. The method of normal modes is a powerful tool[1] if the system is linear and time-invariant. But if the system contains nonlinearities, or has properties which vary in time, the case is much less clear. There is then no mathematical tool of comparable power and generality, and different nonlinear systems require different methods and often special ingenuity. This is especially so when nonlinearity is strong and not merely a small departure from linear behavior.

Musically useful self-sustained oscillators, exemplified by the woodwind, brass, and bowed-string instruments, are often strongly nonlinear. To a large extent, however, they can all be described in terms of conceptually separate linear and nonlinear mechanisms, according to the well-known scheme in Fig. 1. A nonlinear element, such as a reed, air jet, or bow, excites a linear, energetically passive, multimode element such as a tube or string. The linear element in turn influences the operation of the nonlinear element, as suggested by the upper path in Fig. 1.

The nearly periodic nature of self-sustained musical oscillations makes a frequency-domain description seem at first sight more natural than a time-domain description, despite the presence of the nonlinear element. The normal modes of the linear element provide an appropriate framework for such a description, which has indeed proved very useful both in theory and in practice[2,3] especially when the linear element has complicated properties. For example, good shapes for the bores and tone-hole configurations of wind instruments have been determined or rationalized[2–6] by considering the relationships between normal-mode frequencies which favor strong, stable, "mode-locked" regimes of periodic oscillation. Oscillations which are exactly periodic (consisting of frequencies in an exact harmonic series) may

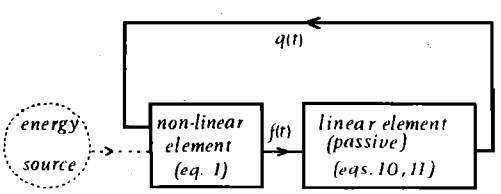

FIG. 1. Block diagram of a fairly general musical oscillator, idealized as an energetically active nonlinear element coupled to an energetically passive linear element.

be possible whatever the natural frequencies of the linear normal modes; but it is plausible that periodic oscillations should be easiest to set up if several of the normal modes have natural frequencies "aligned" in a harmonic series.[2,7] A simple experiment with a violin strikingly illustrates what can happen if this condition is not met.[8] If one of the strings is rendered grossly anharmonic by attaching a small mass at a suitable point—a small paper clip is more than enough—it becomes almost impossible to excite any of the string's graver frequencies by bowing in the usual manner. Wind instruments which similarly refuse to respond can be constructed using bore shapes with anharmonically related normal-mode frequencies, as exemplified by the "tacit horn" of Benade and Gans.[9]

The detailed solution of specific problems using the frequency-domain description is a nontrivial mathematical task, although one that has been pushed to a reasonable conclusion for moderately small amplitudes of oscillation by Worman[10] and Thompson[11] for the clarinet and by Fletcher[12] for the flute or flue organ pipe, and extended to all amplitudes for the clarinet, organ pipe, and bowed string by Schumacher[13–15] and more recently (for the clarinet) by Stewart and Strong.[16] The computations require considerable sophistication. On the whole, the results are in accordance with what one expects intuitively, the fundamental frequency of oscillation usually being a "compromise" such that several of its harmonics lie close to normal-mode frequencies of the linear element.[9] Any normal mode whose resonant bandwidth straddles the fundamental or a higher harmonic of the oscillation frequency is likely to be important. The relationship between actual oscillation frequencies and those of normal modes of the linear element forms a central theme of the important book by Benade.[2] No one has yet succeeded in expressing the relationship in a mathematically precise yet general way, to our knowledge, although a "sum rule" with something of the correct flavor was found in one case.[17] As we shall see, however, a completely general expression of the relationship would have to encompass certain cases where the oscillation frequency turns out, counter-intuitively, to be slightly but systematically *different* from any plausible "compromise" frequency.[15,18,19]

When it comes to transient behavior, the frequency-domain description still gives useful qualitative insights but the computational difficulties are now quite prohibitive. Transients on time scales of the order of tens of milliseconds are well known to be very important for the subjective character of musical sounds. Indeed almost any parameter of the sound signal which is changing on such a time scale is likely to contribute strongly to, and may even dominate, the sound quality perceived by the ear–brain system.[2,20–22] The same time scales are involved in the recognition of consonants in speech. It is no accident that in professional training for musical performance great emphasis is placed on exercises for steadiness of breathing or bowing, and on finesse in the control of such things as attack, articulation, and vibrato.

Such considerations alone would make it desirable to develop the theory of musical oscillators in terms of the time-domain as well as the frequency-domain description. In addition, it is natural to use the time-domain description if one is interested in developing a detailed understanding of the mechanical interactions which occur from moment to moment during a single cycle of oscillation, whether in a steady state or not. Among these are the physical events chiefly responsible for strongly nonlinear behavior, such as the closing of a reed, the onset of slipping of a string past the bow, or the "switching" of an air jet past the lip of a flue organ pipe.

Experience has shown that the time-domain description has another very important advantage. Detailed computations based on it are very much easier to program and carry out, even for steady, periodic regimes of oscillation.[19] It is immaterial whether the nonlinearity is weak or strong. In this paper we illustrate the use of the time-domain description by means of the simplest model that is relevant to common types of nonlinear musical oscillators.

Despite its simplicity this model is remarkably versatile. It can be used to demonstrate essential properties of several physically different types of musical oscillator, showing the extent to which they may or may not be regarded as analogous to one another. Almost any small computer will serve to implement the model. Despite various idealizations the level of realism appears to be commensurate, in some cases, with the accuracy of the best experiments to date, notably the 1976 experiments of Coltman[23] on large-amplitude organ-pipe oscillations. Moreover, it is very easy to extend this type of model to make it as realistic as experimental results are likely to demand in the foreseeable future. Some of the possible extensions will be described, especially for the bowed string, which is the case most thoroughly studied so far.

It is interesting to note that a special case of the model can be reformulated (Appendix A) as an example of a nonlinear difference equation or "iterated map" of the type now being intensively studied for its relevance to chaotic behavior in a variety of physical systems.[24–29] We may expect, of course, that this remark bears more relation to some of the sounds made by novice instrumentalists, than to those normally made by skilled musicians.

I. THE BASIC MODEL

To fix ideas, we begin by thinking in terms of the clarinet. The modifications required to model the violin or flute will be described in Sec. II and Appendix B. In a real clarinet mouthpiece (Fig. 2), a single reed of springy cane controls the rate of flow of air from the player's mouth into the instrument. As a first approximation we may neglect reed dynamics and time-dependent flow control effects. This amounts to assuming that, when the player adopts a given embouchure,

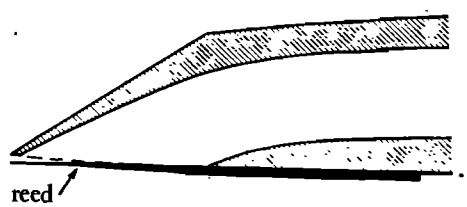

FIG. 2. Cross section of a clarinet mouthpiece. The dashed line shows the "lay" or curved facing that constrains the closing of the reed.

the volume flow rate f, or volume of air flowing through the gap between reed and mouthpiece per unit time, depends only on the pressure drop across the gap at each instant (Ref. 2, Fig. 21.4). Then, for a given pressure p in the player's mouth, f will be a function of p-q only, where q represents the fluctuating pressure just inside the mouthpiece. For notational convenience we suppress explicit reference to p and write this functional dependence simply as

$$f = F(q). \tag{1}$$

For the clarinet the function $F(q)$ behaves roughly as indicated in Fig. 3 by the heavy curve; pressures are measured relative to atmospheric pressure so that q is the usual acoustic pressure. The flow rate f past the reed is counted positive for flow into the instrument. It increases at first as the pressure difference increases from zero (q decreasing from the value p), but then goes to zero again when q reaches some value q_c, say, such that the corresponding pressure drop $p - q_c$ is large enough to overcome the springiness of the reed and close the gap completely. The precise shape of the $F(q)$ curve will evidently depend on embouchure and on the shape of the "lay" of the mouthpiece behind the reed (dashed line in Fig. 2). Realistic $F(q)$ shapes tend to be steeper near $q = p$ than the shape shown, and this has some significant consequences as we shall see.

Of course the finite mass of a real clarinet reed, the inertia in the unsteady air flow through the gap, and the fact that the pressure p in the player's mouth cannot really be constant, all introduce departures from the assumed behavior especially at high frequencies.[2,3,11,30,31] These would be important if we were attempting to describe the finer points of instrument behavior of concern to the musician. Reference 31 shows how to extend the model to take account of the finite mass of the reed, which gives the reed a finite resonant frequency which the player can vary between about 2 and 3 kHz, and whose importance for the subjectively judged tone quality of the clarinet's upper registers has been demonstrated by Thompson.[11] The idealization represented by Eq. (1) does, however, capture the basic nonlinearity, which mathematically speaking is a severe one. The function $F(q)$ shown in Fig. 3 is not only nonlinear, but has a discontinuity in slope at $q = q_c$. Such discontinuities occur in the nonlinear mechanisms of many musical oscillators, and give rise to some of the mathematical difficulties encountered in frequency-domain calculations.

By contrast, the rest of the clarinet and its environment behaves as a linear system to good approximation. Moreover, we can describe that part of the system using standard ideas about wave propagation, an approach that proves to be computationally advantageous. The key idea is to write the acoustic pressure signal $q(t)$ in the mouthpiece as the sum of two contributions representing incoming and outgoing waves, say $q_i(t)$ and $q_o(t)$, where t is time. More precisely, we suppose that there is a section of uniform tube just beyond the mouthpiece, in which the pressure signal takes the one-dimensional form

$$q(x, t) = q_o(t - x/C) + q_i(t + x/C),$$

where x measures distance along the uniform section and C is the sound speed. The associated contributions to the acoustic volume flow rate can be written as

$$Z^{-1}q_o(t - x/C) \text{ and } -Z^{-1}q_i(t + x/C) \tag{2}$$

for the outgoing and incoming waves, respectively, where Z is a real, positive constant, and the acoustic flow rate is counted positive away from the mouthpiece. Z is the wave impedance or characteristic impedance for the uniform section of tube, and is equal to C times air density divided by cross-sectional area.

The linear properties of the clarinet can now be defined in terms of the incoming wave which results from a given outgoing wave. Suppose, for instance, that an infinitely narrow pulse in the form of a Dirac delta function $\delta(t)$ is sent down the tube from $x = 0$ at time $t = 0$, say, so that $q_o(t) = \delta(t)$. Since the tone holes and bell are strong reflectors only for sufficiently low frequencies (below a kHz or so for a real clarinet[32]), the signal returning to $x = 0$ must lose its delta-function character and take on some smooth shape. Let the shape of this hypothetical reflected signal be denoted by $r(t)$; that is,

$$q_i(t) = r(t) \text{ when } q_o(t) = \delta(t). \tag{3}$$

We may call $r(t)$ the "reflection function." It may be thought of as the disturbance that would be found at $x = 0$ after the delta-function pulse is sent out, if the tube were terminated at $x = 0$ by a perfect absorber such as a uniform, semi-infinite tube of the same cross section. Note that considerations of causality imply quite generally that $r(t) = 0$ when $t < 0$.

As a very simple idealization, $r(t)$ might be imagined to look like the inverted hump shown in Fig. 4. For a less simplified "clarinet" with a real bell but no tone holes, $r(t)$ would have a more complicated shape, with several slight undulations following the main pulse. For a real clarinet with some tone holes open the shape would be even more complicated, showing the effects of multiple reflections. Some explicit examples are worked out in Ref. 31. There is no difficulty in allowing for such details, if desired, and for the effects of bore

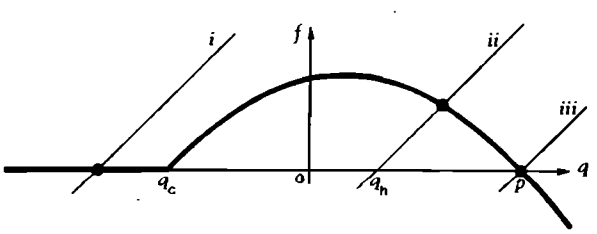

FIG. 3. Heavy curve: Simplified nonlinear characteristic $F(q)$ for a clarinet-like oscillator. The curved part is unrealistically symmetrical; see text near Eq. (24). Sloping straight lines: Eq. (10) for three different values of q_h.

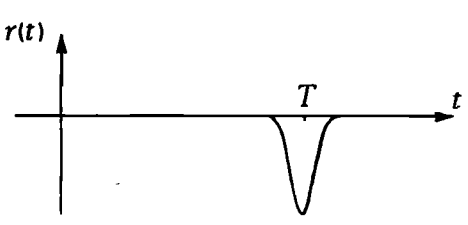

FIG. 4. The simplified reflection function $r(t)$ used in most of our demonstration examples (but cf. Fig. 15).

nonuniformity and acoustic boundary-layer dissipation. One can choose the shape of $r(t)$ to be as realistic as one wants, on the basis of laboratory measurement or theoretical calculation.

Because we are dealing with the linear part of the system, the principle of superposition may be used to write down a general formula for the incoming signal when the outgoing signal has arbitrary time dependence $q_o(t)$ at $x = 0$. The incoming signal $q_i(t)$ is given in general by

$$q_i(t) = r(t) * q_0(t), \tag{4}$$

where the asterisk denotes convolution, defined by

$$r(t) * q_o(t) = q_o(t) * r(t) = \int_0^\infty r(t')q_o(t - t')dt'. \tag{5}$$

Note that according to linear acoustic theory the total area

$$A = \int_0^\infty r(t')dt' = -1, \tag{6}$$

for the reflected pressure signal in any open tube, regardless of the detailed geometry. This expresses the fact that according to linear acoustic theory there can be no permanent, steady difference in pressure between the interior of the tube and the air outside. For, in our notation, the acoustic pressure at the reed is

$$q(t) = q_o(t) + q_i(t). \tag{7}$$

It must tend to zero, after an initial transient, if q_o and the associated flow rate $Z^{-1}q_o$ given by (2) increase from zero to some ultimately steady value, such as it might have if the player were blowing steadily down the instrument with the reed not vibrating. This state of affairs can be described by (4) only if (6) holds [in which case (4) gives $q_i = -q_0$, so that $q = 0$]. In a real clarinet there would in fact be a very small, hydrodynamically induced excess pressure inside the bore, which we are neglecting and which cannot be described by linear acoustic theory. Under conditions of practical interest it is roughly proportional to flow rate squared,[33] and is usually negligible in comparison to the pressure drop *p-q* across the reed, in which we are interested in connection with Fig. 3. This is because the bore is very much larger than the gap between reed and mouthpiece.

All that is now needed to complete the formulation is to note that the acoustic flow rates corresponding to $q_o(t)$ and $q_i(t)$, given by setting $x = 0$ in (2),[34] may be added to give the total acoustic flow rate $f(t)$ at the reed, so that

$$Zf(t) = q_o(t) - q_i(t). \tag{8}$$

Equations (1), (4), (7), and (8) comprise the model equations for the idealized clarinet. They may be given a more compact form by noting that the sum and difference of Eqs. (7) and (8) are, respectively,

$$2q_o = q + Zf \quad \text{and} \quad 2q_i = q - Zf. \tag{9}$$

Substituting these results into (4) we get

$$q(t) = q_h(t) + Zf(t), \tag{10}$$

where

$$q_h(t) = 2q_i(t) = r(t) * \{q(t) + Zf(t)\}. \tag{11}$$

Equations (1), (10), and (11) are almost trivial to solve numerically. If $q(t)$ and $f(t)$ are known at all times earlier than the present, we can step forward in time as follows. First q_h is computed from Eq. (11). It may be thought of as the contribution to q attributable to the past *history* of the system. Any simple numerical approximation to the convolution integral in (11) will do: for a smooth, well-localized $r(t)$ like that in Fig. 4 the trapezoidal rule is as good as any.[35] Then the present values of f and q are found by solving (1) and (10) simultaneously. The time is advanced by a small step Δt and the process repeated. If $r(t)$ is zero or negligible except for a small fraction of an oscillation period, as in Fig. 4, then even the most time-consuming part of the operation, computation of the convolution integral, is quite rapid. Hundreds of cycles of oscillation can be computed in a few minutes on a minicomputer. (Indeed, if the convolution integral were done by hardware using integrated circuits available for the purpose, and the remaining programming done as efficiently as possible in assembly language, a fast minicomputer could produce results at a cycle rate in the audible range. The result would perhaps have some novelty: an electronic musical instrument based on a mathematical model of an acoustic instrument.)

The simultaneous solution of (1) and (10) at each time step, for given q_h, can be visualized graphically as in Fig. 3.[36,37] It corresponds to finding the intersection of the heavy curve representing (1) with the straight line of slope Z^{-1} representing (10). Positions of the straight line are illustrated for three different values of q_h, marked (i), (ii), and (iii). The process of computing the intersection point (q, f) at each time step can be made quite efficient by taking advantage of the fact that q varies monotonically with q_h. We shall assume for the present that $F(q)$ is such that there is only one point of intersection. The consequences of multiple intersections, which are in fact important for the bowed string, will be discussed in Sec. IIC below.

We may want to calculate $r(t)$ from a knowledge of the complex impedance $Z_L(\omega)$ of the linear element, where ω is angular frequency. $Z_L(\omega)$ is defined by

$$Z_L(\omega) = \hat{q}(\omega)/\hat{f}(\omega), \tag{12}$$

where $\hat{q}(\omega)$ and $\hat{f}(\omega)$ are the Fourier transforms of $q(t)$ and $f(t)$, for instance,

$$\hat{f}(\omega) = \int_{-\infty}^{\infty} \exp(-j\omega t) f(t)\, dt. \tag{13}$$

If the transform of $r(t)$ be denoted similarly by

$$\hat{r}(\omega) = \int_0^\infty \exp(-j\omega t) r(t)\, dt, \tag{14}$$

then Eq. (10), using (11) and the convolution theorem, transforms to

$$\hat{q}(\omega) = \hat{r}(\omega)\{\hat{q}(\omega) + Z\hat{f}(\omega)\} + Z\hat{f}(\omega),$$

giving

$$\hat{r}(\omega) = \{Z_L(\omega) - Z\}/\{Z_L(\omega) + Z\}. \tag{15}$$

Taking the inverse Fourier transform gives $r(t)$.

The reflection function $r(t)$ is to be carefully distinguished from the Green's function or impulse response $g(t)$ [which may be defined here as the inverse Fourier transform of $Z_L(\omega)$ itself]. One may describe the linear element in terms

of either, but the computational advantages of working in terms of $r(t)$ rather than $g(t)$ are overwhelming for the type of oscillator under discussion, as was pointed out in Ref. 19. The reason is that $g(t)$ differs significantly from zero over a far longer time interval than $r(t)$, of the order of the decay time of free motion of the linear element, so that the use of $g(t)$ would require computation of an enormously long convolution integral at each time step. Some further discussion concerning this point is given in Ref. 31, and in Appendix B of this paper.

The use of Fourier transforms provides the simplest general way of ensuring that the linear element of the model is energetically passive, since the condition for that to be true is simply that the real part of $Z_L(\omega)$ be positive or zero at all real frequencies ω. In fact we shall require it to be strictly positive for all real, nonzero ω, so that acoustic energy is dissipated, as in actual musical instruments. That is,

$$\mathrm{Re}(Z_L(\omega)) > 0, \quad \text{for } \omega \neq 0, \text{ real.} \tag{16}$$

Equivalently, we require

$$|\hat{r}(\omega)| < 1, \quad \text{for } \omega \neq 0, \text{ real.} \tag{17}$$

This follows from the previous two equations and the fact that the wave impedance Z is a real, positive quantity.

II. SOME EXAMPLES

A. Preliminaries

Even with reflection functions $r(t)$ having very simple shapes, the varieties of behavior that can be produced by solving Eqs. (1), (10), and (11) on a computer are seemingly endless, and are quite reminiscent of the varieties of behavior exhibited by real instruments in the hands of skilled or unskilled players. We present two examples of large-amplitude clarinet-like oscillations involving closure of the reed, and then go on to show how almost the same model can be made to simulate aspects of the behavior of other instruments at various levels of idealization. Included are large-amplitude simulations of a flute or organ pipe which despite the simplicity of the model are actually more realistic, in important respects, than any previously published to our knowledge, with the exception of the (much more elaborate) frequency-domain calculations described in Ref. 14. The latter calculations seem to have been the first to account qualitatively for the triangular waveform observed in the recent organ-pipe experiments of Coltman.[23] Our model produces the same waveforms with far less computational effort, accompanied by greater physical insight.

The reflection function $r(t)$ used throughout most of this paper has the simplified shape shown in Fig. 4, roughly imitating the case of a tube with no tone holes. A Gaussian function

$$r(t) = \begin{cases} a \exp\{-b(t-T)^2\} & (t \geqslant 0) \\ 0 & (t < 0) \end{cases} \tag{18}$$

is chosen for convenience. The constant b is typically chosen so that the full width at value $\frac{1}{2}a$, namely,

$$2b^{-1/2}(\log_e 2)^{1/2}, \tag{19}$$

is 5% to 40% of the round-trip time $T = 2L/C$, L being the effective length of the tube. With these values of b, $r(t)$ is negligible for $t = 0$ (at most $3 \times 10^{-8}\, a$), and so for practical purposes is symmetrical about $t = T$. This will be found convenient for demonstrating certain fundamental points of interest. Strictly speaking the symmetry of $r(t)$ is unrealistic, but the basic behavior to be described is not sensitive to the precise shape of $r(t)$. If we were attempting to describe the finer points of instrument behavior of concern to the musician, then a consideration of the detailed shape would become relevant and indeed vital.

The time step Δt for the simulations is taken as $T/128$ unless otherwise indicated. For the model clarinet (and the bowed string) a is chosen so that the discretized, numerical analog of relation (6) (we used the trapezoidal rule) holds exactly in the simulations. The required values of $r(t)$ were stored in a look-up table, so that the exponentials were evaluated only once.

B. Clarinet-like oscillations

Figure 5 shows waveforms taken from two examples which resemble the large-amplitude behavior of a clarinet. The two examples occupy the left and right halves of the figure. The topmost traces show $q(t)$, and those second from the top the corresponding $f(t)$. It is immediately obvious from the waveforms, which are anything but sinusoidal, that these oscillations are highly nonlinear. As well as using the simple form (18) for the reflection function, these particular examples use the simplest possible analytical representation of the curved part of the nonlinear function $F(q)$, namely the parabola

$$F(q) = k(p-q)(q-q_c), \tag{20}$$

where k is a positive constant. This is the shape actually plotted in Fig. 3, with the numerical values given in the caption to Fig. 5. In the example shown on the left [Fig. 5(a)], the

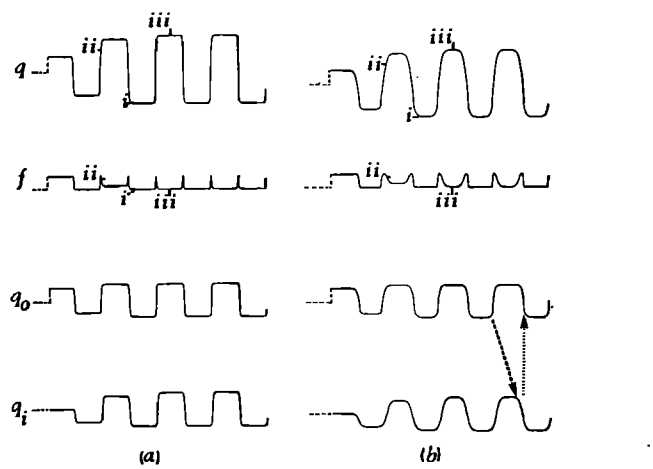

FIG. 5. First few cycles of two clarinet-like oscillations started from rest, obtained by solving Eqs. (1), (10), and (11) with the $F(q)$ shown in Fig. 3. The waveforms of $q(t)$, $f(t)$, $q_o(t)$, and $q_i(t)$ are shown. Values of q and f marked (i), (ii), and (iii) correspond to the positions of the heavy dots in Fig. 3. The left-hand set of waveforms (a) is for a reflection function of full width (19) equal to 5% of the time T for one round trip, or 2.5% of one oscillation period, and the right-hand set (b) is for width 20% of T, or 10% of one oscillation period. Other parameter values (for both sets of waveforms): $k = 0.2$, $p = 3$, $q_c = -2$ in Eq. (20), for $t > 0$, in units such that $Z = 1$; a in Eq. (18) is determined by the trapezoidal approximation to (6). The two sets of waveforms are arranged in columns with the same horizontal time scales, so that simultaneous events occur directly above or below each other.

full width (19) of the reflection function is 5% of the round-trip time $T = 2L/C$ from reed to bell and back. On the right [Fig. 5(b)] it is 20% of T, the broader hump implying a greater loss of high-frequency components during the round trip. This accounts for the more rounded appearance of the right-hand q waveform. To start the oscillations, the blowing pressure p is brought instantaneously from zero to a steady, positive value for $t > 0$ (which is why the initial corner of the waveform is not rounded). Undisturbed conditions, $f = q = 0$, are assumed for $t < 0$. In both examples, the amplitude finally attained is such that the peak positive excursion of q nearly coincides with the right-hand zero of $F(q)$ in Fig. 3, at $q = p = 3$, corresponding to the label (iii) in the figures. The peak negative excursion of q, label (i), goes well to the left of the point $q = q_c = -2$ at which the reed closes completely. In both examples the period is $2T$, or $4L/C$, i.e., two round trips from reed to bell, just as with the lowest note on a real clarinet.

What is happening inside this simplified model "clarinet" can be visualized with the help of the bottom two traces in Fig. 5(a) or 5(b). They show the outgoing and incoming pressure signals $q_o(t)$ and $q_i(t)$, calculated from Eq. (9). Every half-cycle of the periodic oscillation, a pressure jump propagates outward from the reed. Half a period later, it arrives back having been inverted and smeared out by convolution with the reflection function [Eq. (4)]. The smearing can be discerned most easily in Fig. 5(b), by carefully comparing the shapes of each jump in $q_o(t)$ with the corresponding one in $q_i(t)$ half a period later, for instance those joined by the slanting, dashed line.

As the inverted, smeared-out pressure jump arrives back at the reed, it causes the reed to close, if the jump is negative (as in the example just indicated) or to open, if the jump is positive. During this process $q_h(t)$, which is equal to $2q_i(t)$, rapidly traverses the range of values lying between the outermost slanting lines in Fig. 3. The slanting line corresponding to the instantaneous value of $q_h(t)$ therefore sweeps rapidly across the $F(q)$ curve, and if we follow its point of intersection with that curve we see that during the opening or closing of the reed a brief pulse in $f(t)$ is generated. Its peak value corresponds to the peak value of the $F(q)$ curve. The pulse in $f(t)$ adds itself to the smeared-out, incoming pressure jump in such a way as to *steepen* the pressure jump as it sets out again from the reed [see Eq. (8)]. The steepening can again be seen in Fig. 5(b), for instance by comparing the shapes of the incoming and outgoing pressure jumps joined by the vertical, finely dotted line in the figure.

The degree of squareness or roundedness of the periodic $q(t)$ waveform, to which the oscillation settles down, is thus determined by a competition between the smearing described by the reflection function $r(t)$, and the steepening due to the precisely timed puffs of air past the reed represented by the pulses in $f(t)$. A corresponding picture was put forward in 1968 by Cremer and Lazarus[38,39] in the context of the bowed string, which as we shall see shortly is closely analogous. It provides, indeed, an even clearer example of the steepening process. These ideas played an important role in later theoretical developments,[15,18,19,40–43] some of which will be described in the next section and in Appendix B.

A noteworthy feature of Fig. 5 is the rapidity with which the amplitude saturates at its final, steady-state value, in both cases shown. Such very short starting transients recall the metallic hardness of attack which is possible at *fortissimo* levels on a real clarinet. The fast buildup of the oscillation, together with the fact that it saturates at amplitudes for which the maximum positive excursion of $q(t)$ is close to the value p, can be understood from energy considerations, as follows.

In order for self-sustained oscillations to be possible, the mean rate of working W at which energy is supplied to the linear element of the model through the nonlinear element must be positive, by a sufficient margin to balance losses from the linear element. For a periodic oscillation the mean rate of working is

$$W = \langle q(t) f(t) \rangle = \langle q(t) F\{q(t)\} \rangle, \qquad (21)$$

where the angle brackets denote the time average over one period. Positive values of W are made possible by the existence of the positive-sloping part of the $F(q)$ curve, which means that it is possible for $q(t)$ and $F\{q(t)\}$ to be positively correlated in (21). This is sometimes described by saying that the nonlinear element has "negative resistance." Now the waveforms of $q(t)$ and $f(t) = F\{q(t)\}$ in Fig. 5 show that the correlation is very *low* in the final steady state, so that the value of W, although just positive, is numerically much smaller than a product of typical magnitudes of f and q. This condition that the correlation be positive, but only just, largely determines the saturation amplitude under the circumstances of Fig. 5.

The steady oscillations are, moreover, very stable. This is because of the finite negative slope of $F(q)$ at $q = p$, representing locally a *positive* resistance. If the maximum positive excursion of $q(t)$ were to go even slightly beyond the value p, then f and q would become negatively correlated and the oscillation would immediately decay. If on the other hand the positive excursion of $q(t)$ fell significantly short of the value p, then values of W would be closer to the product of typical magnitudes of f and q and therefore much larger than the steady-state value. The amplitude would then grow rapidly. Such large values of W actually occur during the starting transient, as can be seen by visually correlating the first two cycles of the q waveform with those of the f waveform in Fig. 5(a) or 5(b). This accounts for the large initial rate at which the energy builds up in a *fortissimo* attack.

One of the glories of the clarinet as a musical instrument lies in the ease with which a smooth tone can be maintained at extreme *pianissimo* levels, in the low and middle registers. As is well known, this can be accounted for in terms of the control the player has over the operating point on the $F(q)$ curve about which the oscillations take place,[2] and the stability, easily demonstrable in the laboratory,[30,44] of very small amplitude, "threshold" oscillations centered on a point just to the left of maximum $F(q)$, where the slope has just become positive, or the resistance just negative. For a given embouchure, the player can center the oscillation on this part of the $F(q)$ curve merely by decreasing the blowing pressure p to an appropriate value. This corresponds to sliding the $F(q)$ curve rigidly to the left in Fig. 3, keeping k and $p - q_c$ constant,

until the maximum in $F(q)$ falls only just to the right of $q = 0$.

This form of control is effective because the mean value of q itself cannot drift very far from zero. For the model it cannot change at all, for periodic oscillations, since provided (6) holds we can show from the model equations that the mean value

$$\langle q(t) \rangle = 0. \tag{22}$$

To derive this result, note first that for any periodic function $\phi(t)$

$$\langle r(t) * \phi(t) \rangle = r(t) * \langle \phi(t) \rangle$$
$$= \langle \phi(t) \rangle \int_0^\infty r(t)\, dt = -\langle \phi(t) \rangle. \tag{23}$$

The first step follows from the assumption that $\phi(t)$ is periodic, and can be verified by reversing the order of integration, i.e,, by interchanging the average over t with the integration over t', the variable of integration in the convolution. The second step follows immediately from the fact that $\langle \phi(t) \rangle$ is a constant, and the last step from (6), $\int r(t)\, dt = -1$. Applying Eq. (23) to Eq. (11), with $\phi = q + Zf$, we get $\langle q_h \rangle = -\langle q \rangle - Z\langle f \rangle$. Upon substituting this expression for $\langle q_h \rangle$ into the time average of (10) we obtain (22), $\langle q \rangle = 0$.

Now it is an interesting fact that simulations near threshold based on the parabola (20) do *not* exhibit the stable amplitude dependence upon blowing pressure found in the real instrument under normal playing conditions, when the embouchure is not too loose.[44] If p is decreased below its threshold value, then the oscillations die out as expected. However, if p is increased again until small oscillations just grow, then they continue growing until an amplitude is reached at which the model reed begins to close. If small-amplitude oscillations in real clarinets behaved in such an unstable manner, it would require superhuman control to elicit the *pianissimo* sounds which can, in fact, easily be obtained even by a novice.

This unrealistic behavior of the model can be traced to the unrealistic symmetry of the parabola (20). The experiments of Backus[30] on real clarinets suggest an $F(q)$ curve (Fig. 21.4 of Ref. 2) which is much steeper near $q = p$ than it is near $q = q_c$. We could easily use an experimentally determined $F(q)$, but at the present level of idealization it seems adequate to model the asymmetry simply by replacing (20) with a cubic in q such as

$$F(q) = K(p - q)(q - q_c)(q + p - 2q_c), \tag{24}$$

where K is another positive constant. With (24), or any other similarly asymmetric curve in place of (20), the model does indeed exhibit stable, small-amplitude, nearly sinusoidal oscillations, when p is chosen so that the maximum in $F(q)$ falls just to the right of $q = 0$. The stabilization is easily understood in terms of reduced negative resistance as amplitude increases, or more precisely in terms of the effect of the cubic term $-Kq^3$ in (24) upon the rate of working W given by (21). It introduces a new term $-K\langle q^4 \rangle$ into the right-hand side of (21), which is always negative. The dissipation rate in the linear element is proportional to $\langle q^2 \rangle$ as amplitude varies, and so the negative term $-K\langle q^4 \rangle$ always acts to diminish the value of (21), relative to the linear dissipation rate, as oscillation amplitudes increase from zero. It is this that allows a stable balance to be reached within the continuous part of the $F(q)$ curve.

By using a fast Fourier or other routine to Fourier-analyze the waveform of $q(t)$, one can simulate the internal pressure spectrum that would be measured via a probe microphone in the mouthpiece of a real clarinet. It is easy to check that the model reproduces the qualitative behavior of the harmonics shown in Fig. 21.6B of Ref. 2, for instance the proportionality of the third harmonic to the cube of the fundamental as p is varied near the threshold. The even harmonics are relatively weak; but are not, and cannot be, exactly zero, because of the small contribution from $f(t)$ in Eq. (8). The internal spectrum of a real clarinet likewise has weak, but nonzero, even harmonics. It should be noted that the even harmonics would be relatively less weak in the sound radiated from a real clarinet, in comparison to its internal spectrum, for reasons pointed out by Benade (Ref. 2, Sec. 22.4).

C. Pitch flattening in the bowed string

The main nonlinearity in bowed-string dynamics comes from the behavior of the frictional force exerted by the bow on the string. The nonlinearity is even more severe than in the clarinet. One consequence is a phenomenon mentioned briefly in the introduction, namely a systematic shift of the playing frequency away from any plausible "compromise" frequency which might have been expected from an incautious application of frequency-domain ideas to the normal-mode frequencies of the string. The shift occurs whenever the normal force f_b between bow and string exceeds a certain limit, and is downwards, corresponding to a flattening of the pitch. The cause of this interesting phenomenon was not elucidated, to our knowledge, until quite recently.[18,19]

Our simple model can be used as it stands to demonstrate the phenomenon, since the same model equations turn out to comprise an analog of the bowed string. The analogy is a close one if the string is symmetrical and bowed exactly at its midpoint. More generally, one has to allow *inter alia* for reflection from two ends rather than one; details are given in Appendix B. But for a symmetrically terminated string bowed at its midpoint, the two reflections act as one, each half of the string being a mirror image of the other at any instant. The reader who wants to try midpoint bowing on a real instrument should locate the midpoint accurately, degrease the string if necessary, and bow lightly. On some instruments, stopped strings respond better to midpoint bowing than open strings. That the result sometimes sounds a little bit like a faint clarinet may or may not occasion surprise, depending on the extent to which one believes that harmonic content determines tone quality.

The frictional force exerted by the bow on the string plays the same role, in the model, as did the flow rate into the clarinet mouthpiece. It is therefore denoted by the same symbol $f(t)$. The symbols q_o and q_i now represent the transverse string velocities associated with waves traveling out from, and in towards, the bow. Then Eq. (8) applies as before, provided we reinterpret the constant of proportionality Z as equal to half the wave admittance Y of the string. It is admit-

tance and not impedance, because f is now force and not flow rate. Readers who prefer to use the symbol Y for admittance are recommended to substitute $\frac{1}{2}Y$ for Z in Eqs. (8) ff., while reading this section. Note that if f were zero then (8) would imply that $q_o(t) = q_i(t)$, expressing the fact that the outgoing wave in each half of the string would be identical to the incoming wave from the opposite half if the bow were removed.

Equation (4) relates $q_i(t)$ to past values of $q_o(t)$, as before, via a reflection function $r(t)$ with a negative main pulse. This pulse is much narrower for a string of typical length than for the bore of a wind instrument. For demonstration purposes we continue to use the simplified Gaussian form (18) for $r(t)$, although as before $r(t)$ could easily be made more realistic.[45] Note that T in Eq. (18) is the time of a "round trip" over *one half* of the string, not the true round trip over both halves. An advantage of (18) for present purposes is that the almost precisely symmetric shape of $r(t)$ implies that the model string has an almost precisely harmonic series of natural frequencies. Thus there is no difficulty in deciding whether or not the model is exhibiting a nonlinear frequency shift, in the sense asserted.

The sum $q(t)$ of $q_o(t)$ and $q_i(t)$ given by (7) now represents the transverse string velocity at the bow. The relations (6) and (22) still hold, and now express the fact that the string cannot drift continually sideways, which is true when its terminations are modeled in any realistic way.[46] The usual assumption about the friction force,[40,43,47,48] which states that it depends only on the velocity of the string relative to the bow, implies a relation between f and q precisely of the form (1). In summary, therefore, all the model equations, including the final set (1), (10), and (11), are the same as before.

The qualitative appearance of $F(q)$ suggested by existing laboratory evidence[43,47,48] is shown by the heavy curve in Fig. 6. From a mathematical viewpoint this function is vi-

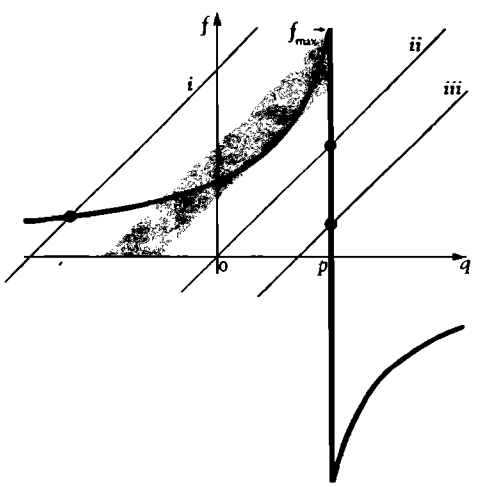

FIG. 6. Heavy curve: Nonlinear characteristic $F(q)$ for the bowed string, idealizing the way in which the frictional force f exerted on the string varies with relative velocity $q - p$, for a bow being pulled or pushed with a given speed p and a given normal bow force f_b. The height f_{max} of the curve is proportional to f_b. Sloping straight lines: Eq. (10) for three different values of q_h; the middle one has $q_h = 0$. The shaded region indicates the range of values of q_h over which the solution (q, f) of (1) and (10) is ambiguous.

ciously nonlinear. It has certain features in common with its counterpart for the clarinet. It again goes through zero at a point $q = p$, say, after attaining a maximum value f_{max}, say, for q just less than p (infinitesimally less, for practical purposes, but see Ref. 48 and Appendix B of Ref. 19); p now represents the velocity at which the bow is being pushed or pulled past the string. For the player, varying p is again an important way of controlling loudness.

Points on the very steep portion of the $F(q)$ curve, where q is very close to p, correspond to the string "sticking" to the bow. In the sticking state, exceedingly small departures from zero relative motion are resisted by relatively large frictional forces. For practical purposes the slope may be regarded as infinite. The maximum value at the peak is roughly proportional to the normal force f_b between bow and string, with a proportionality coefficient of the order of unity for rosined surfaces. Points on the $F(q)$ curve to the left of the maximum represent states of "slipping" with the string moving backwards relative to the bow. Values well to the left of the maximum are typically of the order of $0.2f_b$.

For practical values of f_b, the maximum positive slope of the $F(q)$ curve often exceeds $Z^{-1}(= 2/Y)$, the slope of the straight line representing Eq. (10). An ambiguity then arises in the solution of (1) and (10) for given q_h. This was pointed out (although not resolved) by Friedlander[36] and by Keller.[37] The straight line representing Eq. (10) intersects $F(q)$ at three points, not one, whenever it falls within the shaded region in Fig. 6. A careful analysis of the consequences may be found in Ref. 19, where it is shown that the physically correct resolution of the ambiguity is expressed by the following two statements:

(1) The system will never get into a state corresponding to the middle of the three intersections.

(2) The system follows a given intersection continuously as long as it can.

For instance if the state of the system is currently one of sticking, with the intersection (q, f) on the infinitely steep portion of the curve $F(q)$, then that state will persist (in accordance with the intuitive idea of "sticking") until q_h moves beyond the left-hand edge of the shaded region. Only then will the system jump to a state of slipping. We may say that the bow "releases" the string.[40] Once established, slipping will persist in its turn until q_h leaves the right-hand edge of the shaded region, whereupon a smaller jump will occur, back to the sticking state: the bow "captures" the string. In summary, the sequence of states of the bow-string contact, as $q_h(t)$ oscillates back and forth across the horizontal axis in Fig. 6, exhibits precisely the *hysteresis* which one might have anticipated intuitively. This is very convenient for programming, since the initial guess for q when solving (1) and (10) for given q_h can always be taken as the value of q at the previous time step, and the nearest intersection found. We shall refer to statements (1) and (2) above as the "hysteresis rule."

During the periodic oscillation, the nonlinear interaction between bow and string compensates for the smearing of the waveform described by $r(t)$, in almost the same way as already described for the clarinet. Release of the string corresponds to closing of the reed, and capture of the string to

opening of the reed. The amplitude of steady oscillations is determined in essentially the same way, by the shape of $F(q)$ and in particular by the location of the point $q = p$, which is determined by the bow speed p. However, the waveform-steepening effect of the nonlinear interaction takes a more extreme form whenever hysteresis occurs. Parts of the waveforms of q and f become *infinitely* steep, according to this model, because of the hysteretical jumps in q and f as the straight line representing Eq. (10) sweeps back and forth across the $F(q)$ curve. Moreover, the hysteresis rule implies that the jumps are bigger during release than they are during capture. It is this asymmetry that leads to the downward frequency shift, or flattening effect. The release process introduces a slight delay into the round trip time of the propagating disturbance, which is not fully compensated at capture. How this works in detail will be explained below.

The amount of hysteresis increases as normal bow force f_b is increased, because the $F(q)$ curve then becomes taller and the shaded region wider. The flattening effect therefore increases with f_b, for a given type of oscillation. It also increases with the width of $r(t)$, since incoming signals are then smeared more strongly and there is more scope for perturbing their timing. Precisely these effects occur both in the simulations and on real instruments. On a real violin, audible flattening is easy to demonstrate at low bow speeds when the bow is pressed sufficiently hard onto the string. It becomes audible well before the complete breakdown of the musical note—especially when playing high notes on a thick string such as the *G* string, corresponding to relatively broader $r(t)$.

In practice an audible amount of flattening makes adequate control of pitch, and also of tone quality, impossible for the player. This sets one of the more important limits on the musically useful range of normal bow force f_b. In the light of known results in psychoacoustics, such as those brought out in the perceptive discussions by Boomsliter and Creel[22] and by Benade,[2] it can be anticipated that some of the rapid and irregular frequency fluctuations, which would be caused by the flattening effect under slightly unsteady bowing conditions, might be heard not as pitch fluctuations but as changes in tone quality. From the musician's viewpoint, it is undoubtedly a fact that subjective tone quality tends to *deteriorate* as bow force is increased, even before flattening becomes audible as such; students of violin playing are exhorted not to "force the tone."

Figure 7 shows the $q(t)$ and $f(t)$ waveforms from a steady-state solution to Eqs. (1), (10), and (11) which clearly demonstrates the flattening effect. The parameter values are given in the caption. The oscillations were started from rest, in the same way as for the clarinet [see below Eq. (20)]. The discontinuous jumps in $q(t)$ and $f(t)$ indicating hysteretical behavior are shown dashed in the figure; note that they are respectively larger and smaller for the falling and rising parts of the $q(t)$ waveform, corresponding to the larger jumps at release and the smaller ones at capture. The accompanying pulses in $f(t)$ have correspondingly disparate shapes. If there were no hysteresis, the release and capture pulses would be mirror images of each other, to within numerical accuracy, as are their counterparts in Fig. 5. This follows, in the absence of hysteresis, from the symmetry of our idealized reflection function. The fine dashed extensions to the actual, hysteretical "capture" pulses in $f(t)$ are intended to indicate that the point (q, f) may, if desired, be thought of as instantaneously traversing the peak $F(q)$ value as suggested in Fig. 3 of Ref. 40 and in Fig. 6 of Ref. 15, even though the jump occupies zero time and has no dynamical significance for the model.[49]

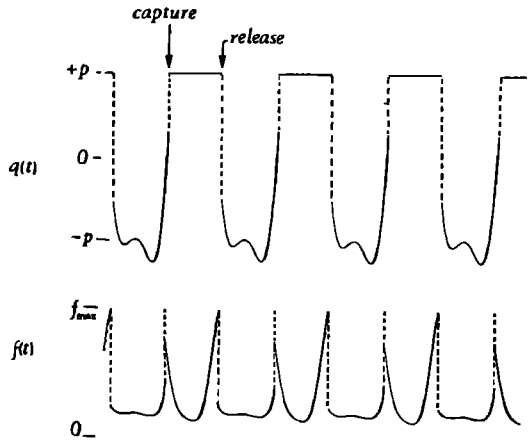

FIG. 7. Waveforms of $q(t)$ and $f(t)$ for a steady-state oscillation, showing a nonlinear frequency shift or "flattening effect" due to hysteresis. The oscillation period is 268 time steps, or 4.7% greater than the string's natural period $2T$ (256 time steps). The waveforms were obtained by solving Eqs. (1), (10), and (11) with the $F(q)$ shown in Fig. 6, and imposing the hysteresis rule to resolve the ambiguity in the shaded region. The left-hand curved part of $F(q)$ has the equation $F(q) = 1/(1.5 - q)$, and the straight part has $p = 1$, so that $f_{max} = 2$, in units such that $Z = 1$. The reflection function has full width (19) equal to 40% of T, or 19.1% of one period; a in Eq. (18) is determined by the trapezoidal approximation to (6).

In this demonstration case, the effects of hysteresis are enhanced by the use of a very broad reflection function $r(t)$, and the flattening effect is quite large. The frequency of oscillation is 4.7% less than the gravest normal-mode frequency, a difference well outside numerical errors. We have flattening by nearly a semitone, "despite" the fact that the linear element in this case has an odd harmonic series of normal-mode frequencies $1/2T$, $3/2T$, $5/2T$, etc. (to within numerical errors), because of the symmetry of $r(t)$. The fact that the normal-mode frequencies comprise an accurately harmonic series can be demonstrated directly, by running the simulation and then continuing it with f set to zero. This gives a nice classroom demonstration of the free decay of the string vibrations when the bow is suddenly raised [cf. the description following Eq. (6) in Ref. 40]. As soon as f is switched off, the frequency jumps up to a value equal to $1/2T$. The waveform becomes more and more rounded as the higher modes decay relative to the lower ones, but shows no dispersion, indicating that all the modes remain in the same phase relation to each other when allowed to decay freely—a situation in which an incautious use of frequency-domain ideas might have predicted that nonlinear self-excitation of the form (1) "should have" produced frequency $1/2T$ or some integer multiple of it.

To see in detail how the flattening effect works, we need only visualize, as before, the consequences of the graphical construction implied by Eqs. (1) and (10), as the straight line

representing Eq. (10) sweeps back and forth across the $F(q)$ curve between its extreme positions, labeled (i) and (iii) in Fig. 6. During release, for instance, when the direction of travel in Fig. 6 is from position (iii) to position (i), q_h has a time dependence like that indicated schematically by the dashed curve in Fig. 8(a). The transition between extreme values is smooth and the rate of change finite because, as noted earlier, q_h is just twice q_i and therefore has the shape of the smeared-out, inverted velocity jump returning to the bow from each end of the string. The corresponding q is indicated by the solid curve. As q_h begins its negative swing, sticking is prolonged while the point (q, f) ascends the infinitely sloping part of the $F(q)$ curve, until the discontinuous jump to a state of slipping occurs. This introduces not only the discontinuity in q, but also an obvious *delay* in the timing of the whole transition in q, relative to that in q_h.

A similar delay appears in the outgoing velocity signal q_o, which is even more strongly affected by the nonlinear interaction. This can be seen from the finely dotted curve in Fig. 8(a), which shows $2q_o$. Its relation to the other two curves is given by

$$2q_o = q + (q - q_h),$$

a consequence of (10) and the first of (9). That is, the graph of $2q_o$ is as far above the q curve as q_h is below it. It is clear by inspection of the graph of $2q_o$ that the nonlinearly induced delay will not be eliminated by the subsequent convolution with $r(t)$. Because of the symmetric shape of $r(t)$, the convolution can only smooth the transition and not make it come earlier. In fact the reverse occurs, since the convolution smears the positive peak in the $2q_o$ curve as well as the main transition. This yields a smooth curve with a smaller peak and an *increased* delay. When this smoothed transition returns, inverted, to the bow, a little more than half a cycle later, it has a shape like that of the dashed curve in Fig. 8(b).

Figure 8(b), in turn, summarizes what happens at capture. The same constructions, with due attention to the hysteresis rule, give the resulting q and q_o curves, again shown solid and finely dotted. The nonlinear interaction now produces an advance in the timing of the transition, rather than a delay. However, because of hysteresis, the advance induced at capture is smaller in magnitude than the delay induced at release. This explains the overall lengthening of the period.

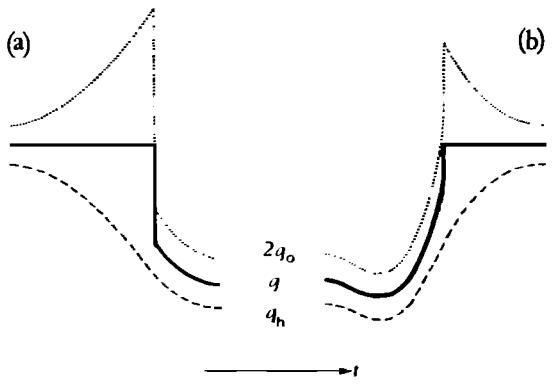

FIG. 8. Sketches showing details in the waveforms, (a) during release, and (b) during capture, of $2q_o(t)$ (shown finely dotted), $q(t)$ (solid), and $q_h(t) = 2q_i(t)$ (dashed), when hysteresis occurs. See text.

D. Subharmonics, starting transients, and other bowed-string phenomena

Our simple model can be used to demonstrate several other nonlinear phenomena characteristic of the bowed string. One such phenomenon is the tendency for subharmonic patterns to occur in starting transients, recently pointed out by Cremer.[50] For midpoint bowing one expects patterns related to the second subharmonic, of period *twice* the string's fundamental period $2T$. Figure 9 shows an example of a decaying second subharmonic pattern, produced by the present model with the same broad reflection function and the same initial conditions as before, but with a gentler $F(q)$ giving no hysteresis (see caption). Decaying subharmonics play an important role in real starting transients, and in other transient phenomena. (An example observed in the laboratory may be seen in Fig. 7 of Ref. 41). Nth subharmonics are liable to occur when the string is bowed near the point $1/N$th of the length of the string from one end. More precisely, it can be shown by a simple geometrical argument[41] that Nth subharmonics are possible when the bow is placed between the points $1/(N+1)$ and $1/(N-1)$ from the end, where $N = 3, 4, 5, \ldots$.

It does not take much experimenting with starting transients before a significant difference between the behavior of the model and that of the real bowed string becomes apparent. As soon as realistically narrow reflection functions are used, transients such as the initial subharmonic in Fig. 9 fail to die out, and stable, steady oscillations become practically impossible to obtain from most initial conditions. This contrasts with the very stable behavior of the model clarinet remarked on earlier, and with the adequately controllable behavior of real bowed strings. The parabola (20) behaves stably, for large-amplitude oscillations, even when it is sufficiently tall or narrow to cause hysteresis, and this actually provides the simplest way of demonstrating the dependence

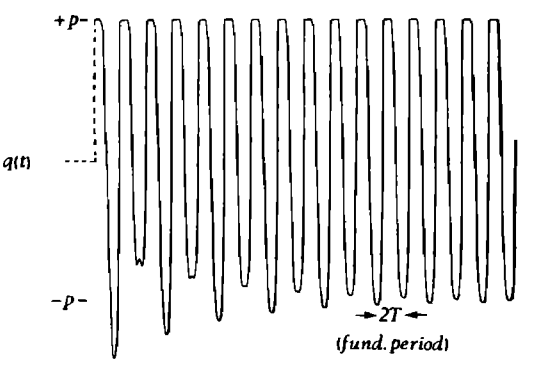

FIG. 9. First sixteen cycles of $q(t)$ in a starting transient, showing a subharmonic pattern. This waveform was obtained with the same parameter values as in Fig. 7, except that the curved part of $F(q)$ is given by $F(q) = 2/(3 - q)$. The straight part again has $p = 1$. (This is a shallower shape than in Fig. 6, and exhibits no hysteresis.) The time step Δt is $T/32$, not our standard value $T/128$. The reflection function again has width (19) equal to 40% of T.

of the flattening effect on the width of $r(t)$ with minimal programming effort.

As these observations suggest, the infinite slope of $F(q)$ at $q = p$ in Fig. 6 is involved in the unstable behavior of the model. Indeed if $r(t)$ is sufficiently narrow, while the sticking part of $F(q)$ has infinite slope and the slipping part finite positive slope as in Fig. 6, it can be shown that even if the simplest regime of steady oscillation were to be set up in the model, that regime would be unstable to small disturbances. The instability was discovered in 1953 by Friedlander[36] for the case of infinitely narrow $r(t)$. It takes the form of a self-excited second subharmonic,[41] which may itself become unstable to a fourth subharmonic, and so on. Such sequences of period doubling bifurcations have recently been studied intensively in other contexts (see Appendix A). The corresponding model for bowing near the $1/N$th point exhibits period N-tupling, if N is a prime number.[51]

This unrealistic behavior does not imply that our treatment of friction, as such, is seriously unrealistic. Sticking is undoubtedly a physical reality, as many experiments have shown clearly. The most important missing ingredient is an entirely different aspect of real string motion, namely the torsional degree of freedom. It is shown in Appendix B that the effects of torsional string motion can be partially taken into account, without changing the model equations or the computer program, simply by replacing the infinitely sloping section of the $F(q)$ curve by a section having finite negative slope.[15] This is just what is needed in order to get realistic, stable transient behavior with narrow $r(t)$. More precisely, the whole friction curve is sheared horizontally, as illustrated in Fig. 10, in such a way as to impart a negative slope $2/Y'$ to the sticking section, where Y' is the torsional wave admittance of the string referred to velocity at the surface of the string. This simple device, albeit not allowing for torsional reflections, does incorporate into the model the scattering of incoming transverse waves into torsional waves at the sticking bow.[43,52] The scattering into torsional waves is by far the most effective mechanism bringing about the decay of subharmonics in real strings.[41]

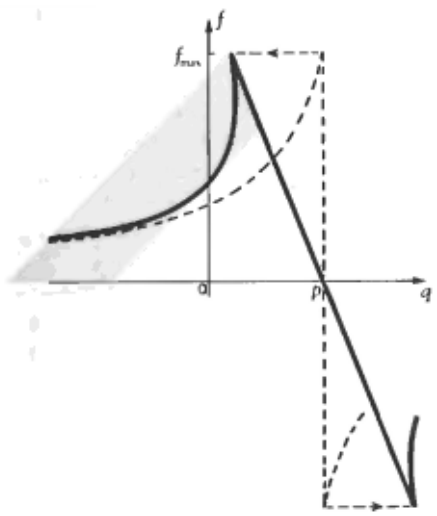

FIG. 10. Solid curve: modified nonlinear characteristic $G(q)$, giving greater stability of oscillation. It is defined by $G(q) = F(q + \frac{1}{2}Y'f)$, where Y' is the characteristic admittance of the string for torsional waves, here taken for illustration as $0.4Y$, a value well within the typical range.[40,43] The dashed curve is the corresponding $F(q)$, identical to that plotted in Fig. 6. Replacing $F(q)$ by $G(q)$ in the model makes some allowance for the scattering of transverse into torsional waves at the bow [Eq. (B16)]. Note incidentally that this gives rise to a larger shaded region and greater hysteresis.[15]

Another characteristic bowed-string phenomenon is the effect of pressing so hard with the bow that no musical note is produced anywhere near the fundamental frequency of the string. This can be simulated simply by increasing f_b and therefore the maximum value of $F(q)$ beyond the limit corresponding to the Schelleng maximum bow force.[53] Then the velocity jumps returning to the bow are not always strong enough to cause release. Both the real string and the model can produce under these conditions a variety of periodic motions with periods much longer than any natural period of the string, as well as apparently aperiodic motions, resembling the particular type of chaotic behavior which in real instruments produces the raucous, scrunching sound sometimes made inadvertently by novice players.

The model is easily extended to describe bowing at any point of an asymmetrically terminated string. Appendix B describes the computationally most efficient way of doing this. The model will then simulate among many other things the celebrated Helmholtz regime, which is actually simpler than the example of Fig. 7 in that only one velocity jump propagates on the entire string, alternately triggering capture and release as it shuttles back and forth past the bow. In the process, backscattered "secondary waves"[38,39,40,43,52] are generated by the accompanying pulses in $f(t)$, and then reverberate in each section of the string (Ref. 41, Fig. 8). The secondary waves have no separate existence in the symmetrical, midpoint case. One can also demonstrate a great variety of other phenomena, including Nth subharmonics, period N-tupling, various "double flyback" motions,[18] and Raman's "higher types" of which our midpoint example, with two propagating velocity jumps, is the simplest case.[54] Contrary to what is sometimes said, Raman's higher types are not unimportant musically.[21,55] Certain of them produce a fascinatingly luminescent sound and are sometimes used, consciously or unconsciously, for coloristic effects in *sul tasto* playing. These particular types tend to be evoked when the bow is near, but not at a point $1/N$th of the length of the string from the bridge, typically when $N = 3$, 4, or 5. The problem of describing and classifying the higher types has recently been approached in a new and interesting way by Lawergren,[55] who uses the term "S motion" to denote the cases just mentioned. General surveys of bowed-string dynamics are given in Refs. 21 and 40, and Ref. 43 gives a more detailed introduction to the subject.

E. Simulating a flute, recorder, or organ pipe

A flue organ pipe open at its far end oscillates with frequency close to $1/T$ or $C/2L$, as does a flute or recorder (blockflute) when playing its lowest note. This is an octave higher than the clarinet's $1/2T$. If a clarinet is played with a flute or recorder mouthpiece substituted, the lowest note goes up about an octave.[56] To model what happens we must take account not only of the altered acoustic conditions at the mouthpiece, but also of the fact that an air jet blowing

across a hole excites acoustic fluctuations, and is affected by them, in an entirely different way from a reed. The geometry of a flue organ pipe is sketched in Fig. 11.

Surprising as it may seem, the same model equations can yet again be shown to be relevant—after making one small but crucial modification to Eq. (1) to be described shortly. In fact the model then appears capable of representing the physical situation to a remarkably good approximation, in the interesting case of large-amplitude oscillations near a strong pipe resonance, about which a great deal is known experimentally.[23,57] Of course $f(t)$ and $q(t)$ again have quite different physical meanings, to be stated shortly, and the nonlinear characteristic $F(q)$ has an entirely different shape.

A full justification of the model equations and their physical interpretation lies beyond the scope of this paper. It would require a lengthy digression, especially as some of the fluid-dynamical questions involved are controversial. Some further discussion will be given in a forthcoming paper.[58] Here we merely present the results, with brief motivation, and then note that the model equations yield excellent simulations of the observed waveforms and phase relations for a large-amplitude oscillation. "Large amplitude" means that the jet switches fully into and out of the pipe.

The modification needed in Eq. (1) arises from the finite speed of hydrodynamical disturbances carried along the jet. These disturbances are the well-known sinuous instability waves first studied by Rayleigh in connection with "sensitive flames" and related phenomena.[59] They travel far more slowly than the speed of sound, usually at speeds of the order of half the maximum flow speed in the jet.[57,60–62] This gives rise to a significant time delay in the process symbolized by the left-hand box in Fig. 1. The importance of the delay is well established experimentally and it is one of the parameters varied by flute players in order to control their instruments.[63] One of its effects is a frequency shift, quite different in nature from the intrinsically nonlinear frequency shift discussed in Sec. IIC: it causes the familiar sharpening of pitch as the instrument is blown harder. To model it in the simplest possible way, Eq. (1) is replaced by a relation of the form

$$f(t) = F\{q(t-\tau)\}, \tag{25}$$

where τ, the delay, is taken to be a positive constant for given playing conditions. We notice that this makes the computer program for solving (10), (11), and (25) even simpler than before, since at each time step the right hand side of (25) is already known in terms of past history, without reference to (10). Therefore (10) need not be solved simultaneously with (25), as it had to be with (1).

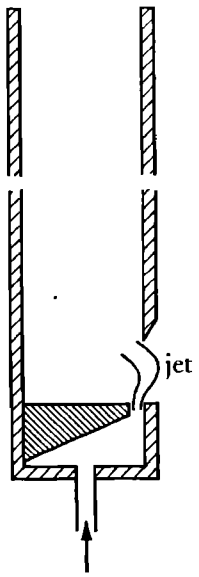

FIG. 11. Flue organ pipe (top and bottom ends shown) with the jet blowing across the mouth, after Cremer and Ising.[57]

The physical meaning of $q(t)$ in this context is that it measures the acoustic displacement of air into and out of the hole across which the jet is blowing. With the example of the flue organ pipe in mind, we shall call this hole the "mouth" of the pipe. Flute players call it the "embouchure hole." For definiteness we take q to be the volume displacement: it has dimensions of length cubed. The corresponding acoustic volume flow rate through the mouth is dq/dt. Positive q will be taken to correspond to displacement into the pipe. Because of the new meaning of q, the sign of the reflection function $r(t)$ is now positive for an open pipe, in the sense that Eq. (6) is replaced by

$$A = \int_0^\infty r(t)\,dt = +1. \tag{26}$$

An open end reflects negatively in terms of pressure, but positively in terms of acoustic flow rate or displacement. [A closed pipe can be modeled by reverting to Eq. (6) and taking $A = -1$.] Strictly speaking, $r(t)$ really represents the cumulative effects of reflection from both ends, as well as the effects of acoustic boundary-layer dissipation. For the sake of definiteness we may think of $q_i(t)$ in Eq. (4) as representing the incoming wave just *after* it has been re-reflected back up the pipe from the mouth, in a hypothetical situation where $f(t)$ is zero. That is, $r(t)$ represents the total smearing of a pulse during a complete round trip. The reflection from the mouth of the pipe may well contribute noticeably to the total smearing of the pulse.[64]

The physical meaning of $f(t)$ is the volume flow rate in that part of the jet which is blowing into the pipe at time t, apart from an additive constant chosen such that the time-averaged value

$$\langle f(t)\rangle = 0 \tag{27}$$

for periodic oscillations. The relation (27) is an exact property of the model, as applied to open pipes, and follows from (26) in the same way as (22) followed from (6). The term $Zf(t)$ in Eq. (8) represents the Cremer–Ising model for the excitation of acoustic disturbances by the jet. The experimental evidence suggests that this is a good model in the near-resonant cases studied by Coltman[23] and by Cremer and Ising.[57] It may be less accurate for strongly blown pipes sounding above resonance.[62] Equation (8), or more conventionally its derivative with respect to time, may be obtained from a consideration of the "excitation" portion of Coltman's (1976) equivalent circuit (Ref. 23, Fig. 9); $f(t)$ and $dq(t)/dt$ correspond, respectively, to i_j and $-i_1$ in his notation. Coltman's equivalent circuit [with the understanding that $\beta x \ll 1$ in his Eq. (1)] represents an aeroacoustically consistent refin-

ement[58] of Cremer and Ising's original model, itself based on a hypothesis due to Helmholtz. The parameter Z in Eq. (8) is no longer a wave impedance or admittance; it has the dimensions of time and equals the time for a sound wave to travel a distance of the same order as the end correction at the mouth of the pipe. It should be cautioned that in the real world the value of Z is not precisely equal to a standard end correction divided by C, nor is it accurately a constant. There is a numerical factor which depends not only on the geometry of the mouth and lip but also in an ill-understood way on the width and speed of the jet, and on the amplitude of the waves on the jet.

An appropriate shape for $F(q)$ in Eq. (25) is a monotonic curve like that shown in Fig. 12, with horizontal asymptotes at each extremity. One extremity of the profile relates to the condition in which all of the jet is blowing into the pipe, and the other extremity to the opposite condition in which the jet is deflected entirely outside it. Following Fletcher and Douglas,[65] we take

$$F(q) = h + k \tanh(lq) \tag{28}$$

in the simulations, where h, k, and l are constants, with l positive and k negative. With the foregoing definitions, it is found experimentally that appropriate values for the delay τ range from just over half an oscillation period (when the pipe is blown gently, and sounds below its resonant frequency), through half a period (at resonance, the regime studied in detail by Cremer and Ising[57] and Coltman[23]), to just over a quarter of a period (when it is blown hard and plays sharp[63,66]). In the more softly blown regimes, the value of τ is of the order of the time for a Rayleigh instability wave to travel to the lip, from the base of the jet where the jet is most acoustically sensitive.[59] In hard-blown regimes the behavior of the jet is less simple; a good discussion of the theoretical and experimental evidence on jet behavior may be found in the papers by Fletcher and Thwaites.[60–62] The reason for taking k negative in (28) is explained in Refs. 3, 57, 60, and 62: when jet instability is important the response of the jet to $q(t)$ is almost the same as if q were zero but the slit from which the jet emerges was moving from side to side in the opposite sense,[67] with displacement $-q(t)$.

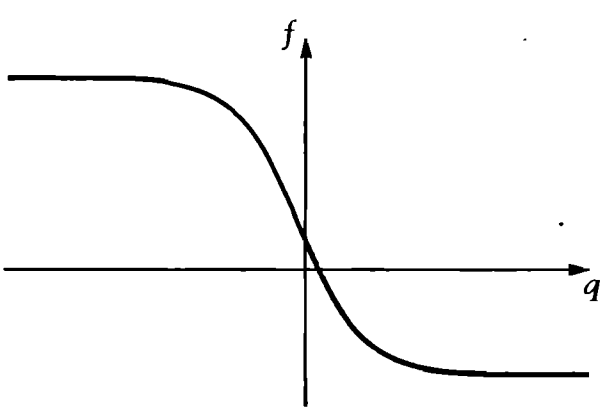

FIG. 12. Nonlinear characteristic $F(q)$ for a flute-like oscillator [Eq. (25)]. The model assumes, see (29), that the value of f is determined by the value of q at a time τ in the past, crudely imitating the propagation delay for Rayleigh instability waves on the jet.

The assumption, implicit in the assumed form of (25), that jet behavior depends only on $q(t)$, is itself valid provided that typical magnitudes of $f(t)$ and $dq(t)/dt$ satisfy

$$f(t) \ll dq(t)/dt. \tag{29}$$

In real organ pipes there is a local contribution, $-f(t)$, to the volume flux in the mouth, which (25) neglects so far as its effect on the base of the jet is concerned. This is a good approximation in cases of large-amplitude pipe oscillations near resonance. The neglected contribution represents a local, irrotational backflow out of the mouth, which occurs for reasons of mass conservation whenever the jet blows into the mouth. It would be the *only* irrotational contribution to the flow in the mouth if the interior of the pipe were blocked making $dq(t)/dt$ zero.[68] The backflow and the effective mass-acceleration associated with it are actually an essential part of the Cremer–Ising mechanism expressed by Eq. (8), and must be considered carefully in any theoretical determination of the magnitude of the coefficient Z; but its direct effect upon the excitation of instability waves at the base of the jet can be neglected if (29) holds. This approximation would not be appropriate if we wished to simulate the transition from edge-tone to pipe-tone behavior so beautifully demonstrated by Coltman.[23] The direct effect of $-f(t)$ upon the base of the jet is the feedback mechanism giving rise to edge-tone behavior.

There are yet other reasons, not least the strong frequency dependence of the growth rates of instability waves, why Eq. (25) is in principle a far cruder idealization for the organ pipe than Eq. (1) is for the clarinet or the violin. Fortunately, however, the inaccuracies inherent in (25) are almost completely immaterial for the case of large-amplitude, near-resonant oscillations that interests us most. In that case, not only is (29) well satisfied, as will now be illustrated (and as can also be verified directly from Coltman's[23] experimental results by comparing his Figs. 7 and 8), but the jet moreover spends most of its time fully "switched" into or out of the pipe, so that $f(t)$ is very nearly a square wave (again as reported by Coltman). That is, the system spends most of its time on one or other of the asymptotes in Fig. 12, and is indifferent to details in the waveform of the acoustic displacement $q(t)$ and in the form of (25), except near zero crossings.[69] In addition, the waveform of $q(t)$ tends to be weak in high harmonics, so that the frequency dependence of the growth rates of instability waves is of less consequence than might at first be thought.

Figure 13 presents an example of steady-state waveforms obtained from Eqs. (10), (11), and (25), using the idealized reflection function $r(t)$ given by (18). Numerical values are given in the figure caption. The parameter h of the nonlinear characteristic (28) is zero (unlike Fig. 12). In virtue of (27), $h = 0$ corresponds to a time-average jet position exactly bisected by the lip, so that no even harmonics are generated.[65,66] As well as the waveforms of q and f, we show, in the correct relative phase, those of dq/dt and df/dt together with those of the outgoing and incoming signals dq_o/dt and dq_i/dt computed from Eq. (9). They are the most useful waveforms for making a comparison with the experimental results reported by Coltman.[23] The scale on which dq/dt is

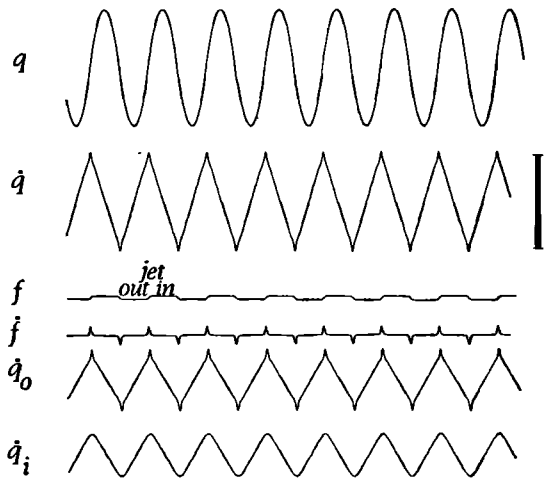

FIG. 13. Waveforms for a steady-state, flute-like oscillation exactly at resonance ($\tau = T/2$), obtained by solving Eqs. (10), (11), and (25). The waveforms of q, dq/dt, f, df/dt, dq_o/dt, and dq_i/dt are shown. Positive volume displacements and velocities are directed into the mouth or embouchure hole of the pipe, and positive f means that the jet is blowing into the pipe. The vertical bar on the right gives the theoretical peak-to-peak amplitude of dq/dt for the limiting triangular waveform discussed in Ref. 58. This peak-to-peak value is 3.84, corresponding to positive and negative excursions $\pm$ 1.92. The reflection function has full width (19) equal to 15% of T. Other parameter values (for both sets): $h = 0$, $k = -0.5$, $l = 0.2$ in (28); $Z = 0.0233T$; a in Eq. (18) is determined by the trapezoidal approximation to (26).

plotted is the same as for f, to give some idea of the accuracy of the approximation (29). The results of Fig. 13 were obtained by stepping Eqs. (10), (11), and (25) forward in time until steady oscillations were obtained. To get the oscillation started, a small, constant displacement q was assumed to exist before turning on the jet.

The time delay τ is one half the round-trip time T, and the period of the resulting steady oscillations is $T = 2L/C$, precisely that of the pipe's gravest free mode. The model pipe is oscillating precisely at resonance. The delay $\tau = T/2$ required for this differs from the value $\tau = 3T_e/4$ characterizing the gravest edge-tone oscillation of period T_e.[70] Resonance does not mean that the edge-tone frequency agrees with the pipe frequency, as has sometimes been assumed. The reason is the different delay in the feedback mechanism producing edge tones, via the local backflow $-f(t)$ instead of the acoustic pipe flow dq/dt.

The waveforms and phase relations shown in Fig. 13 are strikingly consistent with all the observations reported by Coltman[23] for oscillations in a long organ pipe at resonance. In particular, Coltman remarked on the triangular shape of the experimental dq/dt waveform, as well as on the square waveform of f and on the experimentally determined phase relation between them (jet switches into mouth, i.e., f goes positive, at the time of maximum dq/dt, i.e., at maximum acoustic flow into the mouth). Coltman also remarked on the waveform of pressure at different positions within the pipe, finding a triangular waveform at the midpoint and trapezoidal waveforms at positions in between the midpoint and the ends. The observations showed that the entire pressure distribution $P(x,t)$ "takes very closely the form of the wave on a string plucked in the middle." All these features are reproduced by the expression

$$P(x,t) \propto \frac{\partial}{\partial t} q_o\left(t - \frac{x}{C}\right) - \frac{\partial}{\partial t} q_i\left(t + \frac{x}{C}\right), \qquad (30)$$

which estimates $P(x,t)$ for a uniform pipe in terms of the outgoing and incoming signals, neglecting boundary-layer dissipation and any other contribution to $r(t)$ that may originate from the body and mouth of the pipe, rather than at the far end. The waveforms implied by (30) at any given x can easily be constructed by suitably phase-shifting the bottom two waveforms in Fig. 13 and subtracting the result graphically. For instance, at the midpoint the two contributions reinforce to give the same triangular waveform as dq/dt, but delayed by a quarter period relative to dq/dt itself. At other values of x they combine into a trapezoidal waveform.

A partial explanation of the triangular shape of the dq/dt waveform was given in Ref. 14 from a frequency-domain viewpoint. The time-domain viewpoint leads to a much more complete explanation (which, once perceived, is easy to translate into frequency-domain language). In fact one can show that an approximately triangular waveform is to be expected, at resonance, *irrespective of the shape of* $r(t)$, as long as $r(t)$ is sufficiently narrow, and as long as the jet is switching. This interesting theoretical result seems not to have been remarked upon previously. It shows that the waveforms we have found can probably be regarded as a genuine explanation of Coltman's result, even though we do not know the exact shape of $r(t)$ for his experiment. It should apply in practice to any relatively long pipe with sufficiently small acoustic losses.

The derivation of this theoretical result is given in mathematical detail in Ref. 58. Its basis is essentially the principle described earlier (and first used by Cremer[39] for the case of the bowed string), namely that the shape of the steady-state waveform can be understood in terms of a competition between the sharpening of its corners by the pulses in df/dt [Eq. (8)], and their smearing-out by $r(t)$ [Eq. (4)]. Note that, as before, the incoming waves dq_i/dt in Fig. 13 (bottom trace) have rounder corners than the outgoing waves dq_o/dt (second from bottom). However, there are essential differences as compared to the clarinet and bowed string. These differences are related to the different shape of the nonlinear characteristic. The $F(q)$ shape shown in Fig. 12 cannot exert strong nonlinear control over the steady-state amplitude in the manner of the $F(q)$ shapes shown in Figs. 3 and 6. Once the jet is switching fully into and out of the pipe, $f(t)$ becomes nearly a square wave, whose amplitude is insensitive to the amplitude of q. The amplitude of q is therefore limited mainly by dissipation, represented in the model by the properties of $r(t)$. This fact, and the triangular shape of the waveform itself, can also be understood in terms of an analogy with a simple problem in heat diffusion.[58]

The important role of linear dissipation in the model helps us to undertand another aspect of its behavior not mentioned until now, namely the length of the starting transient. The starting transient predicted by the model (not shown) is very much longer than, say, for the model clarinet at large amplitude. This is also true in the real world, where the flute is known as one of the slowest-speaking members of the or-

chestra, despite the compensating skills developed by flautists. The duration of the model transient, which exhibits a smooth, monotonic growth of amplitude, is of the same order as the time for the gravest mode of the linear element to decay freely. We shall not discuss the model's starting transients in detail, since for one thing the approximation (29) is unlikely to hold in the earliest stages of such a transient. In addition, if we were aiming at realistic transients we would have to pay closer attention to the actual nonlinear fluid dynamics,[71,72] implying possible variations in Z during the transient.[58] In a real starting transient, moreover, the jet orifice may act momentarily as an isolated monopole. This seems likely to be important for getting the oscillation going, especially if the note is vigorously "tongued" by the player.

The model as it stands successfully imitates various other real-world phenomena. Varying the delay to a fourth, a sixth, and an eighth of the round trip time T results in oscillations at frequencies of two, three, and four times the fundamental, simulating the flautist's or recorder player's production of the octave, twelfth, and second octave by "overblowing," i.e., increasing jet speed and reducing the delay τ. Variation of τ between these simple integral fractions produces the frequency-shifting effects already mentioned. The introduction of even harmonics by displacing the jet off-center, most recently discussed by Fletcher and Douglas[65] and by Nolle,[66] may easily be simulated, in the present case of an open pipe, by making h nonzero. This displaces the $F(q)$ curve vertically, imitating one of the ways in which a flute player can vary tone quality, or an organ builder "voice" an open flue pipe. Note incidentally that because (27) constrains $\langle f \rangle$ and not $\langle q \rangle$ to be zero for the open pipe, shifting the $F(q)$ curve horizontally would exert essentially no control over the conditions of oscillation: $\langle q \rangle$ would simply shift by the same amount, and other details would be unaffected. This is consistent with the intrinsic arbitrariness in the choice of an origin for the displacement q in an open pipe. The reverse is true for a closed pipe; it is now $\langle q \rangle$ that is zero, as for the clarinet, and control must be exerted (in the model at least) by shifting the $F(q)$ curve horizontally. It is not actually obvious how to choose the shift *a priori* in either case; the time-average position of the jet in the real instrument involves nontrivial fluid-dynamical effects, not accounted for in the model, of which the "acoustic streaming" associated with boundary-layer dissipation is only one example.[73–75] It is simplest to regard the imposed shift in the $F(q)$ curve as a disposable parameter to be chosen for consistency with observed behavior.

III. CONCLUDING REMARKS

The simple time-domain model defined by Eqs. (10), (11), and (25), supplemented where necessary by the hysteresis rule described in Sec. IIC, has been found capable of mimicking basic aspects of the strongly nonlinear behavior of the clarinet, violin, and flute families simply by changing the shapes of the functions $r(t)$ and $F(q)$ which characterize the linear and nonlinear elements of the model, and by changing the time delay τ in Eq. (25) (zero for the clarinet and violin, and positive, usually of the order of half an oscillation period, for the flute family).

Three basic phenomena which are reproduced by the model and which are easy to understand from a time-domain viewpoint are

(1) the frequency shift which can be caused by a sufficiently severe nonlinearity $F(q)$, of practical significance for the bowed string (Sec. IIC),

(2) the nonlinear amplitude-limiting mechanism for clarinet and bowed-string oscillations, tightly controlled by the shape of $F(q)$ (Secs. IIB, C), and

(3) the entirely different amplitude-limiting mechanism in the flute family, controlled mainly by dissipation in the linear element and hardly at all by the shape of $F(q)$ (Sec. IIE). This helps explain the tendency of the flute family to exhibit relatively long starting transients.

These and many other phenomena are modeled in a qualitatively correct way even when using the simplified reflection functions $r(t)$ and nonlinear characteristics $F(q)$ suggested here for demonstration purposes and ease of programming.

When implementing time-domain models it is generally useful to arrange for the parameters of the simulation to be varied interactively from the computer keyboard while the simulation proceeds. The simulation can then be "played," more or less as a real instrument is played. A little experience with this soon reminds one of a well-known property of nonlinear phenomena, namely their nonuniqueness. Several different regimes may be possible for the same final set of parameter values, especially for $F(q)$ shapes like that in Fig. 6. One soon learns how to encourage a given type of oscillation during the initial transient, a matter in which musicians develop superlative skill. One is also reminded of the rich variety of periodic and aperiodic behavior which may be exhibited by even the simplest nonlinear oscillators (see Appendix A). The question of which behaviors are physically realistic for musical-acoustical purposes, and which result from too unrealistic a choice of model characteristics, has yet to be studied systematically, although instructive examples regarding stable versus unstable behavior were encountered in Secs. IIB and IID.

It is easy to extend the simple time-domain model presented here to other instruments, and to the more elaborate levels of simulation needed for direct comparison with laboratory data. We have found such models extremely useful in our research on the bowed string[18,19,41,42] and on the clarinet.[31] When finite reed mass is taken into account, as in more refined models of the clarinet which allow for the reed resonance,[11,31] an integro-differential system of equations takes the place of the simple integral system solved here, but the equations are still amenable to efficient numerical solution by stepping forward in time.[31] This modification is essential in the case of the brass wind instruments, for which "reed" or lip mass is of leading importance.[3,76] Integro-differential equations also arise naturally for the oboe and other conical-bore instruments, because of the inertia of the air near the small end of the bore. Conical-bore instruments can be modeled by replacing (2) with the corresponding formulae for spherical waves.[73]

The bowed string, by contrast, can be simulated very realistically with models which are direct extensions of the present one, involving integral equations only. In our inves-

tigations into the many observed regimes of periodic and aperiodic bowed-string behavior, time-domain simulations have proved extremely helpful in achieving a definitive interpretation of laboratory results. The key to constructing an efficient algorithm is to introduce more than one reflection function.[19] "Right-hand" and "left-hand" reflection functions $r_R(t)$ and $r_L(t)$ are used to characterize the shapes of pulses returning to the bow from the two ends of the string, as described in Appendix B. Moreover, for any quantitative simulation of real strings, or even a *qualitatively* correct simulation of starting transients and other transient behavior, it is vital to take torsional as well as transverse motion into account as was noted in the discussion following Fig. 9 (Sec. IID).

An interesting bowed-string phenomenon easily studied by these methods is the "wolf note." Two wolf simulations are shown in Fig. 14. They were obtained by solving Eqs. (B13)–(B14) and (1) using a Gaussian right-hand transverse reflection function of the type shown in Fig. 4, but realistically narrow, and a left-hand transverse reflection function of the type shown in Fig. 15, having a similar main pulse followed by a weak, decaying oscillation representing the effect of a damped resonance in the left-hand string termination. These examples are classical "simple" wolves of the kind first explained by Raman in 1916,[21] for which the resonant period of the string termination is close to the full round-trip time T for the two string sections taken together. Here the resonant period of the string termination is $65T/64$.

A point of special interest is that the only parameter changed between the two simulations was the normal bow force f_b; see captions to Figs. 14–16 for further detail. The simulations thus illustrate the fact that the wolf or "beat" period may increase substantially (by a factor of about 3/2 in this case) as f_b increases (by a factor 2 in this case). Further simulations, not presented here, showed that the increase is monotonic as f_b varies. The increase in wolf period is easily understandable from Raman's explanation, which was based on time-domain thinking and the concept of "mini-

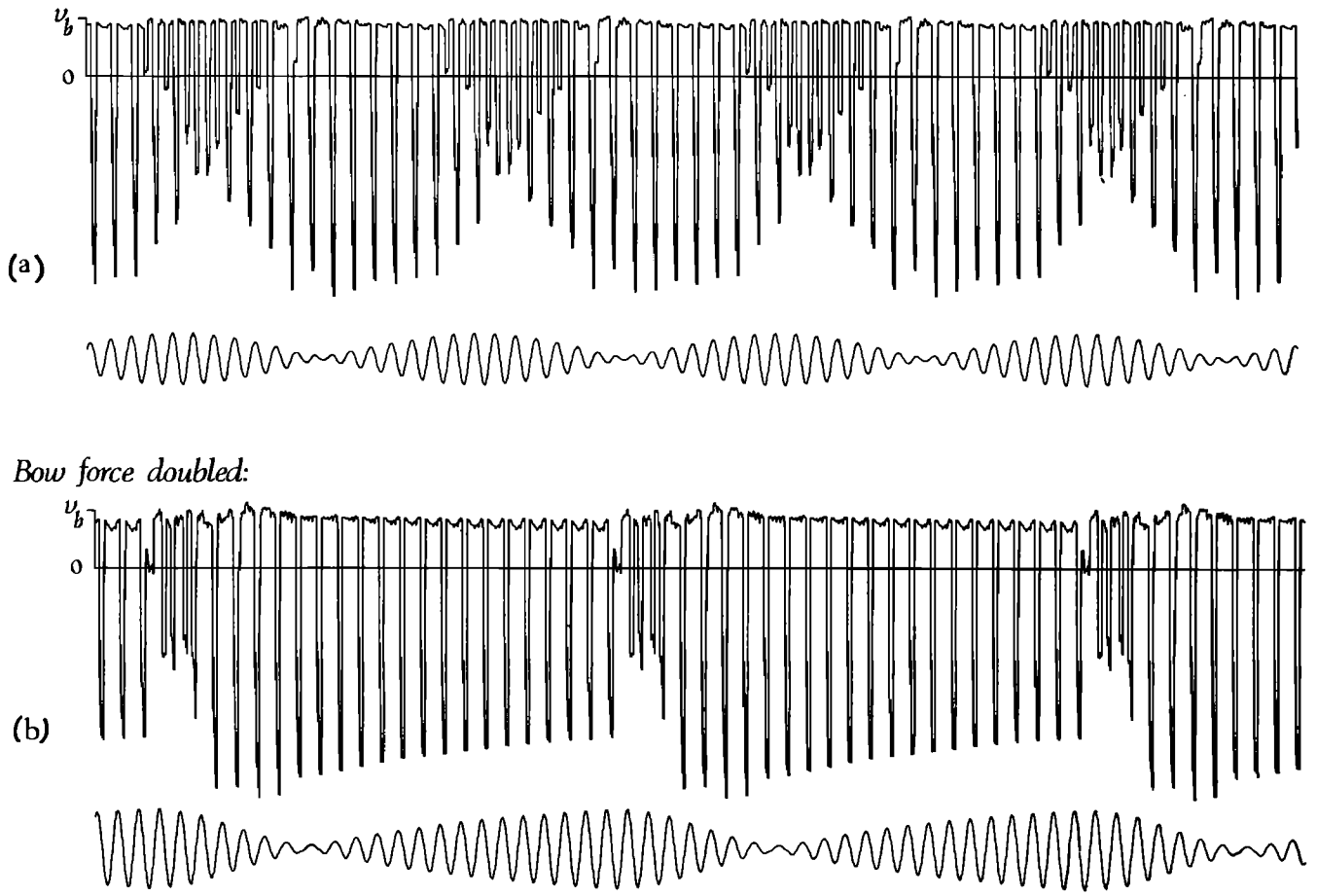

FIG. 14. Two simulated wolf notes, from Eqs. (B13) and (B14) and (1), illustrating the variation of wolf period with normal bow force f_b. Bow force for the lower pair of traces is double its value for the upper pair. All other parameters are the same for the two wolves. Waveforms shown are transverse center-of-mass string velocity at the bow (upper waveforms), and bridge velocity on the same scale (lower waveforms). The right-hand reflection function has full width (19) equal to 3.9% of the round-trip time T for the whole string [$b = (128/3T)^2$ in (18), the same as in Fig. 9 of Ref. 19; note incidentally that $\sqrt{3}/128$ and $(2/3)^{1/2}$ in that caption are wrong and should be 3/128 and 2/3, respectively, and similarly that 1.5 in the caption to Fig. 18 of Ref. 41 should be 1.5^2]. The time step Δt is $T/128$ and the propagation delays for transverse waves on the left- and right-hand sections of string are in the ratio 24:104, so that the bow is nominally 3/16 of the way along the string. The main pulse of the left-hand reflection function also has width 3.9%, and the parameters for the oscillatory tail are specified in the caption to Fig. 15 below. The torsional and transfer reflection functions are set to zero. The nonlinear characteristics $F(q)$ used in Eq. (1) are those shown in Fig. 16. They correspond to values $1.2v_b$ and $2.4v_b$ of normal bow force f_b, in units such that $\frac{1}{2}Y = 1$, where $v_b (= p)$ is the bow speed and Y is the transverse wave admittance of the string. The ratio Y'/Y of torsional to transverse wave admittance is 0.2.

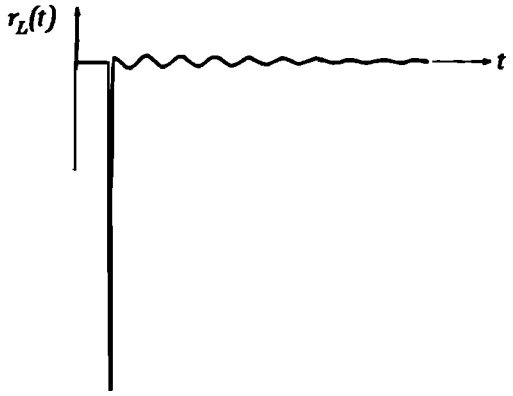

FIG. 15. Left-hand or "bridge" reflection function of the type needed for simulating wolf notes, from Ref. 19, with a main pulse centered on $t = T_L$ and a decaying tail proportional to the real part of $\exp[(j\omega - \omega/2Q)(t - T_L)]$, representing the effect of free motion of the bridge. In the example shown the free decay has a Q of 30; the same Q value is used for the simulations in Fig. 14. The amplitude of the bridge motion is governed by the admittance ratio $Y^{-1}(SM)^{-1/2}$, where S and M are the effective stiffness and mass seen by the string at the bridge[77] and Y is the transverse wave admittance of the string; here $Y^{-1}(SM)^{-1/2}$ is 0.05 to make the decaying oscillation clearly visible, but the more realistic value 0.01 is used for the simulations in Fig. 14. The main pulse is a Gaussian whose full width is 3.9% of the round-trip time T for the whole string. When computing the convolution integral, efficiency is gained by separately computing the contributions from the main pulse and from the decaying sinusoid, and using the fact that the latter contribution to the integral, in complex form, is equal to the corresponding quantity already computed at the previous time step, multiplied by $\exp[(j\omega - \omega/2Q)\,\Delta t]$, plus a further contribution from the current time step.

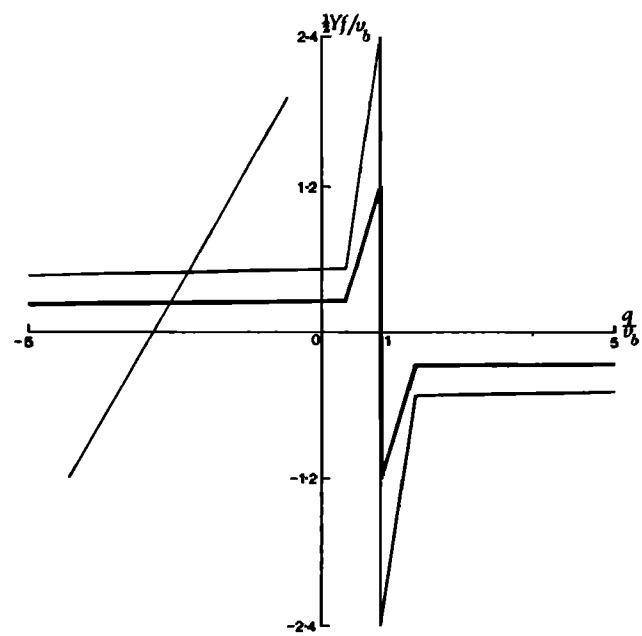

FIG. 16. The two nonlinear friction characteristics $F(q)$ used in the wolf-note simulations, made up of straight line segments as a computationally convenient approximation. Here q is velocity of the string surface at the bow, and $v_b (= p)$ is bow speed. It is assumed, in qualitative agreement with laboratory evidence,[43,47,48] that $F(q)$ scales with normal bow force f_b, so that the heavy $F(q)$ corresponds to the upper pair of traces in Fig. 14, and the light one to the lower pair of traces in Fig. 14, with double the value of f_b. The straight line represents Eq. (B13), for one value of $q_h = (q_{iL} + q_{iR} + q'_{iL} + q'_{iR})$. Its slope is $(1 + Y'/Y)^{-1} = 0.83$, in terms of the dimensionless units marked on the axes.

mum bow force."[21,40,43] The simplest frequency-domain explanation of the wolf note[77] fails to predict the increase, since it associates the wolf period with properties of the linear element alone. The linear properties are identical in the two simulations shown.

The progress achieved so far using the time-domain approach poses a stiff challenge to the ingenuity of experimenters in musical acoustics today. There is now no mathematical nor computational impediment to running extremely realistic and detailed simulations of musical oscillators, which could lead to quantitative comparisons with experiment, and ultimately to simulations sophisticated enough to be useful as practical design tools in musical instrument manufacture. At present the main impediment to such progress is a lack of high-precision experiments yielding sufficient information about real reflection functions and nonlinear characteristics. In some cases, special ingenuity may be required to obtain the relevant information. For instance, to measure all the relevant reflection functions for a real bowed-string instrument (see Appendix B) the surface as well as the center-of-mass motion of the string has to be excited and observed. Moreover the measurements will have to be done at extremely high spatial and temporal (or phase) resolution, in order to observe the kind of detail in the transverse and torsional reflection functions which is relevant to the very fast events characteristic of the nonlinear bow-string interaction.

ACKNOWLEDGMENTS

We thank A. H. Benade, A. C. Pay, and K. Gough for helpful discussions or correspondence on the clarinet family, B. J. Bayly, A. H. Benade, J. Coltman, J. E. Ffowcs Williams, H. Ising, and N. H. Fletcher on the flute family, and L. Cremer on bowed-string starting transients. Professor Benade and Professor Cremer kindly read the first draft of the paper and made a number of perceptive comments, leading to a greatly improved presentation. JW acknowledges support from the Department of Engineering and from Clare College, Cambridge, RTS support from the National Science Foundation under Grant PHY-8007431, and MEM support from the Nuffield Foundation under Grant SCI/168/92 for work on jet-drive fluid dynamics.

APPENDIX A: RELATION TO THE THEORY OF ITERATED MAPS

It is the purpose of this appendix to show that Eq. (10) can be written under some conditions as a nonlinear difference equation or "iterated map" (cf. Refs. 36 and 37) of a type that has been extensively studied in recent years. The equation to be derived is

$$g_j = AH(g_{j-1}), \tag{A1}$$

where $H(g)$ is a nonlinear function of g with a single quadratic extremum in the domain of the argument, and A is a constant. The case $H(g) = g(g - 1)$ is one simple example. The general behavior of such equations for different values of A has been reviewed by May.[24] Recent advances of interest to physicists have been published by Feigenbaum,[26] and an overview is given in a recent monograph by Collet and Eck-

mann.[25] One motivation for these theoretical developments lies in the possible connection between the solutions of Eq. (A1) and the onset of "turbulence" or chaotic behavior in less simple systems. The behavior predicted by Feigenbaum has indeed been found in systems more complicated than those for which the theorem has been proved, for instance in certain fluid-dynamical systems.[27–29]

Suppose the reflection function is a delta function $r(t) = A\delta(t - T)$. We now drop the requirement that $A = -1$. Then in units such that $Z = 1$, Eq. (10) becomes, with (11),

$$q_n = A(q_{n-1} + f_{n-1}) + f_n, \tag{A2}$$

where q_n is the value of $q(t)$ for t between nT and $(n+1)T$. All the time-dependent functions are constant for each round-trip period T, changing their values instantaneously only at times T later than the last change. Corresponding to $2q_i$ and $2q_0$ in (9), define

$$g_n = q_n - f_n \tag{A3}$$

and

$$h_n = q_n + f_n. \tag{A4}$$

As just defined, h appears to depend on both q and f. However, if specifying g uniquely determines q, then $h = H(g)$, and the problem takes the form of Eq. (A1). As long as the maximum positive slope of $F(q)$ is less than unity (no hysteresis), then g does uniquely determine q.

With an $F(q)$ like that shown in Fig. 3, and A negative, $AH(g)$ has a single quadratic minimum at a positive value of g. Feigenbaum's conditions[26] are satisfied. From a theoretical viewpoint the interest lies in how the period of the oscillations depends on A. We have done computer simulations of the system represented by Eq. (A1), using an $F(q)$ of the type shown in Fig. 3, and found the expected succession of period doublings as A is decreased towards -1, following quantitatively the universal behavior predicted by Feigenbaum. With an $F(q)$ of the type shown in Fig. 6, the model becomes the Raman model of a string bowed at its midpoint. As indicated in Sec. IID, we still get sequences of period doublings. These have a different asymptotic behavior, as expected from the fact that the extremum in $H(g)$ is no longer quadratic. For some $F(q)$ curves there are ranges of A for which the period is very large (often exceeding the time of the simulation), and for which the spectrum is very complicated, occasionally even resembling broadband noise. All these phenomena persist when we take $r(t)$ to have small but finite width.

APPENDIX B: MORE REALISTIC MODELS OF THE BOWED STRING

The first step in generalizing the model is to allow for an asymmetrically terminated string bowed at any point. The most efficient algorithm is obtained by introducing separate reflection functions $r_L(t)$ and $r_R(t)$ for the sections of string to the left and right of the bow, respectively.[19] The functions $r_L(t)$ and $r_R(t)$ are a concise means of describing the effects of the left- and right-hand string terminations, together with the propagation delay, high-frequency attenuation and wave dispersion on each section of the string. The terminations may be of any kind, provided that both they and the string behave linearly. Note incidentally that $r_L(t)$ and $r_R(t)$, which were called "corner-rounding functions" in Ref. 19, were defined there with sign and time-origin conventions differing from those used here.

Equation (1) is unaltered,

$$f = F(q), \tag{B1}$$

but Eq. (4) is now replaced by the pair

$$q_{iL} = r_L * q_{oL}, \quad q_{iR} = r_R * q_{oR}, \tag{B2}$$

Eq. (7) by

$$q = q_{oL} + q_{iL} = q_{oR} + q_{iR}, \tag{B3}$$

and Eq. (8) by

$$\tfrac{1}{2}Yf = q_{oL} - q_{iR} = q_{oR} - q_{iL}, \tag{B4}$$

where $q_{oL}(t)$ and $q_{iL}(t)$ represent the outgoing and incoming velocity waves to the left of the bow, $q_{oR}(t)$ and $q_{iR}(t)$ those to the right of the bow, and where the constant Y is the wave admittance of the string. As was remarked in Sec. IIC, admittance plays the same mathematical role for the bowed string as impedance does for the clarinet, owing to the different physical meanings of $q(t)$ and $f(t)$. Here q is the transverse velocity of the string at the bow (whereas it was mouthpiece pressure for the clarinet), and f is the friction force exerted on the string (whereas it was flow past the reed for the clarinet). The first of Eqs. (B4) expresses the fact that the wave going out to the left is the same as the wave coming in from the right, apart from an additional contribution due to the friction force f. The effect of f is to generate additional velocity waves $\frac{1}{2}Yf$ which radiate equally in both directions away from the bow. The implied symmetry manifests itself in the invariance of (B4) under exchange of suffices L and R.

Equations (B1)–(B4) are complete but not all independent, since the right-hand equalities in (B3) and (B4) are equivalent to each other. The equations may be rearranged to give a complete and independent set preserving the formal symmetry between L and R, and convenient for numerical solution. Subtracting (B4) from (B3) gives

$$q = (q_{iL} + q_{iR}) + \tfrac{1}{2}Yf, \tag{B5}$$

which may be compared to (10). Use of (B4) to eliminate q_{oL} and q_{oR} from (B2) gives

$$q_{iL} = r_L * (q_{iR} + \tfrac{1}{2}Yf), \quad q_{iR} = r_R * (q_{iL} + \tfrac{1}{2}Yf), \tag{B6}$$

which may be compared to (11). Equations (B1), (B5), and (B6) can evidently be solved numerically in just the same simple way as before, with $(q_{iL} + q_{iR})$ playing the role of q_h and representing the contribution to $q(t)$ attributable to past history. This is what was done in Ref. 19. At each time step, (B6) is used to compute the new values of q_{iL} and q_{iR}, and then (B1) and (B5) are solved simultaneously to get the new values of q and f. As was shown in detail in Ref. 19, the Friedlander–Keller ambiguity, if it occurs, is to be resolved using the hysteresis rule stated in Sec IIC.

The next major step towards realism is to allow for torsional string motion. As was pointed out in Sec IID, torsional waves are highly significant for the way in which a real string responds to the bow, especially during any kind of transient. Equations (B2)–(B4) generalize to

$$q_{iL} = r_L * q_{oL} + s_L * q'_{oL}, \quad q_{iR} = r_R * q_{oR} + s_R * q'_{oR}, \tag{B7}$$

$$q'_{iL} = r'_L * q'_{oL} + s'_L * q_{oL}, \quad q'_{iR} = r'_R * q'_{oR} + s'_R * q_{oR}, \tag{B8}$$

$$q = q_{oL} + q_{iL} + q'_{oL} + q'_{iL} = q_{oR} + q_{iR} + q'_{oR} + q'_{iR}, \tag{B9}$$

$$\tfrac{1}{2}Yf = q_{oL} - q_{iR} = q_{oR} - q_{iL}, \tag{B10}$$

and

$$\tfrac{1}{2}Y'f = q'_{oL} - q'_{iR} = q'_{oR} - q'_{iL}. \tag{B11}$$

Here $q_{iL}(t)$, etc., denote the transverse center-of-mass velocity signals at the bow, and $q'_{iL}(t)$, etc., the torsional angular velocities multiplied by string radius, i.e., normalized so that the total surface velocity $q(t)$ at the bow is given by simple summation, Eq. (B9). It is the surface velocity $q(t)$, rather than the center-of-mass velocity, $q_{oL} + q_{iL}$ or $q_{oR} + q_{iR}$, that governs the friction force $f(t)$ through Eq. (1). The torsional-to-transverse "transfer" reflection functions $s_L(t)$, $s_R(t)$ appearing in Eqs. (B7) are related to their transverse-to-torsional counterparts $s'_L(t)$, $s'_R(t)$ in (B8) according to

$$Ys'_L(t) = Y's_L(t), \quad Ys'_R(t) = Y's_R(t), \tag{B12}$$

by the reciprocal theorem.[78] Y and Y' are, respectively, the transverse and torsional wave admittances of the string, referred to surface velocity and force. According to measurements by Schelleng,[40] typical values of Y'/Y lie in the range 0.26 to 1 (the value 0.2 used for the wolf notes in Fig. 14 being somewhat on the low side, but still enough to attenuate transient subharmonics quite effectively[41]). Experimental information on torsional and transfer reflection functions is lacking; the latter would seem unlikely to be very important for a string fitting snugly into a bridge notch, but might be more significant, perhaps, when the other end is stopped by the player's finger, under which the string might roll. Like transverse waves, torsional waves travel with little dispersion. They travel several times faster, depending on the type of string,[40,43,47] and so torsional reflection functions may be expected to be dominated by narrow pulses with shorter delays.

Once again, a more concise form of the equations may be derived. Equation (B5) is replaced by

$$q = (q_{iL} + q_{iR} + q'_{iL} + q'_{iR}) + \tfrac{1}{2}(Y + Y')f \tag{B13}$$

[cf. (10) again], and Eqs. (B6) by

$$q_{iL} = r_L * (q_{iR} + \tfrac{1}{2}Yf) + s_L * (q'_{iR} + \tfrac{1}{2}Y'f), \tag{B14a}$$

$$q_{iR} = r_R * (q_{iL} + \tfrac{1}{2}Yf) + s_R * (q'_{iL} + \tfrac{1}{2}Y'f), \tag{B14b}$$

$$q'_{iL} = r'_L * (q'_{iR} + \tfrac{1}{2}Y'f) + s'_L * (q_{iR} + \tfrac{1}{2}Yf), \tag{B14c}$$

$$q'_{iR} = r'_R * (q'_{iL} + \tfrac{1}{2}Y'f) + s'_R * (q_{iL} + \tfrac{1}{2}Yf). \tag{B14d}$$

In applying the hysteresis rule, it should be remembered that the straight lines in Figs. 6 and 16 now represent Eq. (B13), and so have slope $\{\frac{1}{2}(Y + Y')\}^{-1}$, or $(1 + Y'/Y)^{-1}$ in units of $\frac{1}{2}Y$. Thus torsion always increases hysteresis.[15]

In connection with the discussion in Sec. IID, we note that if all disturbances associated with torsion are assumed (somewhat unrealistically) to be perfectly absorbed by the string terminations, as in the example of Fig. 14, then the problem becomes mathematically the same as the problem without torsion, provided we replace the $F(q)$ of Eq. (1) or (B1) by the nonlinear function $G(q)$ of Fig. 10. For if all torsional and "transfer" reflection functions are set to zero, then the right-hand sides of (B14c) and (B14d) vanish, Eqs. (B14a) and (14b) reduce immediately to (B6), and (B13) reduces to an equation of the same *form* as (B5),

$$\tilde{q} = (q_{iL} + q_{iR}) + \tfrac{1}{2}Yf, \tag{B15}$$

where we have defined $\tilde{q} = q - \frac{1}{2}Y'f$. Since $F(q) = G(\tilde{q})$, by definition of G, we have

$$f = G(\tilde{q}) \tag{B16}$$

in place of Eq. (B1), showing that the problem has precisely the same mathematical form as the problem without torsion, with $\tilde{q}$ playing the role of q, and $G(\tilde{q})$ the role of $F(q)$. $G(\tilde{q})$ may well be multiple-valued, but the hysteresis rule still applies exactly as stated in Sec. IIC.

Equations (B13) and (B14) may be generalized still further to allow for real, nonrigid bow hair,[15,79] in which case reflection functions for longitudinal waves on the bow hair are introduced. These involve time delays which vary in a prescribed manner as the bow moves past the string. The measured properties of bow hair imply that the associated effects should be smaller than those associated with torsional string motion.[43,47,79] Another degree of freedom of real strings is transverse string motion normal to the bow hair, which is coupled to the main transverse motion parallel to the bow hair via the string terminations and also, nonlinearly, via bow-hair friction.[80–82] Normal bow force f_b then becomes a time-dependent variable rather than a prescribed parameter, and reflection functions for transverse waves on the bow hair are required. The fact that the hair is bent through a small but finite angle at the string, for finite f_b, may also need to be taken into account. It is not known to what extent generalizations of this type, some of which go far beyond what is known experimentally, are musically important.

A different kind of generalization, which recently helped us to identify a prominent source of audible noise in bowed-string sound,[42] is to allow the string to be bowed at two or more neighboring points simultaneously. This enabled us to simulate the "differential slipping" of the string past a bow of finite width. Under certain parameter conditions it proved to be the main cause of audible noise, particularly when the string is bowed very close to one end. It is often quite significant under conditions encountered in concert performance, and sets one of the practical limits on the usable range of f_b.

Some of the foregoing generalizations represent conceptual elaborations as well as elaborations of detail, since they involve schemes more complicated than that shown in Fig. 1. For instance, in the case of the string bowed at two points simultaneously there are now two nonlinear elements, linked to a linear element with two inputs and two outputs.

When implementing models of the form indicated by Fig. 1, it might be asked why the simpler-looking equations (10) and (11) are not used instead of (B5) and (B6) and their further generalizations. For Eqs. (10) and (11) still hold if we *define* a single "reflection function" $r(t)$ through (15).[31] The latter definition applies formally to any linear element with one input $f(t)$ and output $q(t)$. The numerical method needs no modification if $r(t)$, so defined, is zero or bounded in the neighborhood of $t = 0$, since in that case q_h as defined by (11)

still depends only on the past history of the system. This can be shown to be true of any model in which the impulse response $g(t)$ of the linear element begins with a narrow, isolated spike at $t = 0$ which can be approximated as a delta function, as discussed in Ref. 19, but is finite thereafter. The parameter Z appearing in Eq. (15), or $\frac{1}{2}Y$ in (B5), must be set equal to the area under the initial spike. The approximation of the initial spike by a delta function is related to the basic assumption of Sec. I, that a separation into sets of incoming and outgoing one-dimensional waves is possible. Now $r(t)$ usually decays much more rapidly than $g(t)$,[31] because of a cancellation of poles in (15), leading to a gain in computational efficiency over the direct use of $g(t)$. However, the computational efficiency obtainable when separate reflection functions are used is far greater still. This is the reason why (B5) and (B6) and their various extensions are to be preferred.

[1]Lord Rayleigh, *The Theory of Sound* (Dover, New York, 1945), Vol. 1.
[2]A. H. Benade, *Fundamentals of Musical Acoustics* (Oxford U.P., New York, 1976).
[3]N. H. Fletcher, "Air flow and sound generation in musical wind instruments," Ann. Rev. Fluid Mech. **11**, 123–146 (1979).
[4]A. H. Benade, "On woodwind instrument bores," J. Acoust. Soc. Am. **31**, 137–146 (1969).
[5]C. J. Nederveen, *Acoustical Aspects of Woodwind Instruments* (Frits Knuf, Amsterdam, 1969).
[6]R. A. Smith and G. J. Daniell, "Systematic approach to the correction of intonation in wind instruments," Nature **262**, 761–765 (1976).
[7]H. Bouasse, *Instruments à vent* (Librairie Delagrave, Paris, 1929), Vol. I, pp. 68–79.
[8]Reference 2, Sec. 23.6.
[9]A. H. Benade and D. J. Gans, "Sound production in wind instruments," Ann. N. Y. Acad. Sci. **155**, Art. 1, 247–263 (1968).
[10]W. Worman, "Self-sustained oscillations of medium amplitude in clarinet-like systems," Ph.D. dissertation, Case Western Reserve University, Cleveland, OH, 1971.
[11]S. C. Thompson, "The effect of the reed resonance on woodwind tone production," J. Acoust. Soc. Am. **66**, 1299–1307 (1979).
[12]N. H. Fletcher, "Sound production by organ flue pipes," J. Acoust. Soc. Am. **60**, 926–936 (1976).
[13]R. T. Schumacher, "Self-sustained oscillations of the clarinet: an integral equation approach," Acustica **40**, 298–309 (1978).
[14]R. T. Schumacher, "Self-sustained oscillations of organ flue pipes: an integral equation solution," Acustica **39**, 225–238 (1978).
[15]R. T. Schumacher, "Self-sustained oscillations of the bowed string," Acustica **43**, 109–120 (1979).
[16]S. E. Stewart and W. J. Strong, "Functional model of a simplified clarinet," J. Acoust. Soc. Am. **68**, 109–120 (1980).
[17]Reference 14, Eqs. (38) and (47).
[18]M. E. McIntyre, R. T. Schumacher, and J. Woodhouse, "New results on the bowed string," Catgut Acoust. Soc. Newsletter **28**, 27–31 (1977).
[19]M. E. McIntyre and J. Woodhouse, "On the fundamentals of bowed-string dynamics," Acustica **43**, 93–108 (1979).
[20]E.g., H. Fletcher and L. C. Sanders, "Quality of violin vibrato tones," J. Acoust. Soc. Am. **41**, 1534 (1967). See also (for instance) J.-C. Risset and M. V. Mathews, "Analysis of musical instrument tones," Physics Today **22**(2), 23 (1969), and the earlier work of H. Fletcher, E. D. Blackham, and O. N. Geertsen, "Quality of violin, viola, cello and bass viol tones," J. Acoust. Soc. Am. **37**, 851–863 (1965).
[21]M. E. McIntyre and J. Woodhouse, "The acoustics of stringed musical instruments," Interdiscipl. Sci. Rev. **3**, 157–173 (1978).
[22]P. C. Boomsliter and W. Creel, "Research potentials in auditory characteristics of violin tone," J. Acoust. Soc. Am. **51**, 1984–1993 (1972).
[23]J. W. Coltman, "Jet-drive mechanisms in edge tones and organ pipes," J. Acoust. Soc. Am. **60**, 725–733 (1976).
[24]R. M. May, "Simple mathematical models with very complicated dynamics," Nature **261**, 459–467 (1976).
[25]P. Collet and J.-P. Eckmann, *Iterated Maps on the Interval as Dynamic Systems* (Birkhäuser, Boston, 1980).
[26]M. J. Feigenbaum, "Quantitative Universality for a class of nonlinear transformations," J. Stat. Phys. **19**, 25–52 (1978).
[27]P. R. Fenstermacher, H. L. Swinney, S. Benson, and J. P. Gollub, "Bifurcations to periodic, quasiperiodic, and chaotic regimes in rotating and convecting fluids," Ann. N.Y. Acad. Sci. **316**, 652–666 (1979).
[28]A. Libchaber, C. Laroche, and S. Fauve, "Period doubling cascade in mercury, a quantitative measurement," J. Phys. (Paris) **43**, L211–216 (1982).
[29]D. R. Moore, J. Toomre, E. Knobloch, and N. O. Weiss, "Period doubling and chaos in partial differential equations for thermalsolutal convection," Nature **303**, 663–667 (1983).
[30]J. Backus, "Small amplitude vibrations of the clarinet," J. Acoust. Soc. Am. **35**, 305–313 (1963).
[31]R. T. Schumacher, "Ab initio calculations of the oscillations of a clarinet," Acustica **48**, 72–85 (1981).
[32]Reference 2, Fig. 22.9, points marked "E_3."
[33]E.g., *Modern Developments in Fluid Dynamics*, edited by S. Goldstein (Dover, New York, 1965), Sec. 167. We have ignored an additional, weak logarithmic dependence.
[34]The precise placing of the x origin to imitate a real clarinet depends of course on the geometry of the mouthpiece. It also depends on the finite compliance of the reed, which provides a way in which the player can control tuning (Ref. 30, Fig. 1).
[35]M. Abramowitz and I. Stegun, *Handbook of Mathematical Functions* (Dover, New York, 1965), Eq. (25.4.7).
[36]F. G. Friedlander, "On the oscillations of a bowed string," Proc. Cambridge Philos. Soc. **49**, 516–530 (1953).
[37]J. B. Keller, "Bowing of violin strings," Comm. Pure Appl. Math. **6**, 483–495 (1953).
[38]L. Cremer and H. Lazarus, "Der Einfluss des Bogendrucks beim Anstreichen einer Saite," Proc. 6th ICA Congress on Acoustics, N9–N12 (Tokyo, 1968).
[39]L. Cremer, "Der Einfluss des 'Bogendrucks' auf die selbsterregten Schwingungen der gestrichenen Saite," Acustica **30**, 119–136 (1974).
[40]J. C. Schelleng, "The bowed string and the player," J. Acoust. Soc. Am. **53**, 26–41 (1973).
[41]M. E. McIntyre, R. T. Schumacher, and J. Woodhouse, "Aperiodicity in bowed-string motion," Acustica **49**, 13–32 (1981); see also Ref. 42.
[42]M. E. McIntyre, R. T. Schumacher, and J. Woodhouse, "Aperiodicity in bowed-string motion: on the differential-slipping mechanism," Acustica **50**, 294–295 (1982).
[43]L. Cremer, *Physik der Geige* (Hirzel Verlag, Stuttgart, 1981). (English translation to be published by MIT Press.)
[44]For too loose an embouchure it is found experimentally that the stability of the oscillations is lost.[30]
[45]In a model with sufficiently high temporal resolution, one could easily include such features as the oscillatory precursors to the main pulse which are evident, for instance, in the experimental data shown in Fig. 2(b) of Ref. 19. These precursors are manifestations of wave dispersion due to the bending stiffness of the string. See also Appendix B.
[46]But it should be noted that (6) and (22) fail when pure-resistive string terminations are used, as in the celebrated Raman model of the bowed string,[15,43,54] for which $r(t)$ is a delta function with area $|A| < 1$.
[47]L. Cremer, "Die Geige aus der Sicht des Physikers," Nachr. Akad. Wiss. Göttingen: II Math. Phys. K1. **12**, 223–259 (1971).
[48]See, e.g., E. Rabinowicz, "Stick and Slip," Sci. Am. **194**(5), 109–118 (1956).
[49]It is probably insignificant for real bowed strings as well, for a somewhat different reason.[19] Although jumps which are exactly instantaneous would not take place in reality, the idealization $f = F(q)$ is itself highly unlikely to be applicable at this point. The friction force probably never reaches the maximum value of $F(q)$ during capture. Thus the fine dashed extensions in the $f(t)$ waveform in Fig. 7 are probably more indicative of the properties of the *model* than of the physical reality.
[50]L. Cremer, "Consideration of the duration of transients in bowed instruments," Catgut Acoust. Soc. Newletter **38**, 13–18 (1982), Fig. 6. See also the English version of Ref. 43.
[51]J. Woodhouse, "On the acoustics and mechanics of stringed musical instruments," Doctoral thesis, University of Cambridge, Cambridge, England, 1977.
[52]L. Cremer, "Das Schicksal der 'Sekundärwellen' bei der Selbsterregung von Streichinstrumenten," Acustica **42**, 133–148 (1979).

[53]Reference 40, Eq. (2), with the right-hand side multiplied by 2 as indicated in footnote 10 of the same reference. Schelleng's result was derived assuming Helmholtz motion in a string bowed near one end, and an $F(q)$ shape like the heavy curve in Fig. 6. More generally, one may define the Schelleng maximum f_b, for a given periodic oscillation, as the value of f_b which makes the peak in $F(q)$ too tall to permit release. In this (strongly hysteretical) situation the shaded region in Fig. 6 overlaps the left-hand excursion of the assumed oscillation, implying that the assumed regime of oscillation cannot in fact exist. So defined, the Schelleng maximum is an upper bound on the possible values of f_b for the given type of oscillation. In the present case the oscillation breaks down well before this bound is reached.

[54]C. V. Raman, "On the mechanical theory of vibrations of bowed strings," Indian Assoc. Cult. Sci. Bull. No. 15, 1–158 (1918).

[55]B. Lawergren, "On the motion of bowed violin strings," Acustica **44**, 194–206 (1980).

[56]Professor Benade writes that this is a "favorite lecture demonstration" of his; see Ref. 2, Sec. 22.6.

[57]L. Cremer and H. Ising, "Die selbsterregten Schwingungen von Orgelpfeifen," Acustica **19**, 143–153 (1967).

[58]M. E. McIntyre and R. T. Schumacher, "On the triangular waveforms observed in long organ flue pipes at resonance," to be submitted to J. Acoust. Soc. Am.

[59]Lord Rayleigh, *The Theory of Sound* (Dover, New York, 1945), Vol. 2, Article 370.

[60]N. H. Fletcher and S. Thwaites, "Wave propagation on an acoustically perturbed jet," Acustica **42**, 324–334 (1979).

[61]S. Thwaites and N. H. Fletcher, "Wave propagation on turbulent jets," Acustica **45**, 175–179 (1980); see also S. Thwaites and N. H. Fletcher, "Wave propagation on turbulent jets. II. Growth," Acustica **51**, 44–49 (1982).

[62]N. H. Fletcher and S. Thwaites, "The physics of organ pipes," Sci. Am. **248**(1), 84–93 (1983).

[63]N. H. Fletcher, "Acoustical correlates of flute performance technique," J. Acoust. Soc. Am. **57**, 233–237 (1975).

[64]A more accurate model could be constructed in which separate reflection functions are used for reflection from the mouth and from the far end, just as for the model of an asymmetrically bowed string formulated in Appendix B.

[65]N. H. Fletcher and L. M. Douglas, "Harmonic generation in organ pipes, recorders, and flutes," J. Acoust. Soc. Am. **68**, 767–771 (1980).

[66]A. W. Nolle, "Adjustments affecting the steady waveforms of flue organ pipes," J. Acoust. Soc. Am. **73**, 1821–1832 (1983).

[67]The two situations can be shown to be dynamically equivalent if: (a) the local jet hydrodynamics is incompressible (which is true to an extremely good approximation for the low Mach number jets we are concerned with), and (b) the transverse acoustic displacement is locally a rigid, bulk motion across the base of the jet, and the acoustic pressure gradient locally uniform in space (roughly true at best, depending on the geometry of nearby boundaries—e.g., Fig. 11). Given (a) and (b), one can transform the hydrodynamical equations from an inertial to a transversely accelerating frame of reference, in which the acoustic pressure gradient is just balanced by the "fictitious force" due to the acceleration, and the fluid is locally at rest apart from the jet issuing from a transversely oscillating orifice.

[68]In Coltman's equivalent circuit (Ref. 23, Fig. 9), this contribution is represented by the contribution i_j to the total current in the short end of the transmission line representing the mouth of the pipe.

[69]In the opposite extreme of small amplitude (so small that the instability waves behave linearly all the way to the lip), a more realistic model could be achieved by inserting an appropriate *bandpass filter* into the upper path in Fig. 1, thus mimicking selective amplification of jet displacements by Rayleigh instability waves. (This refinement would be especially important in any extension of the model to simulate edge-tone behavior.)

[70]The edge-tone delay τ is not $5T_e/4$, as has sometimes been concluded from attempts to measure the nonuniform, difficult-to-observe spatial structure of the growing waves on the jet (and also from theoretical arguments in which mistakes concerning phase relations were made). Coltman's[23] direct and intrinsically more reliable measurements of *temporal* phase relations show clearly that the time delay on the jet for the gravest edge-tone of period T_e is $3T_e/4$. (Note that Coltman's quoted phases are for transverse jet displacements at the lip referred to transverse velocity, not displacement, at the base of the jet; see discussion in Ref. 60.)

[71]J. E. Ffowcs Williams and L. H. Hall, "Aerodynamic sound generation by turbulent flow in the vicinity of a scattering half plane," J. Fluid Mech. **40**, 657–670 (1970).

[72]J. H. M. Disselhorst and L. van Wijngaarden, "Flow in the exit of open pipes during acoustic resonance," J. Fluid Mech. **99**, 293–319 (1980).

[73]E.g., M. J. Lighthill, *Waves in Fluids* (Cambridge U.P., Cambridge, 1978).

[74]A. H. Benade and W. B. Richards, "Second-harmonic sound generation at woodwind tone holes," J. Acoust. Soc. Am. Suppl. 1 **71**, S91 (1982).

[75]M. E. McIntyre, *Waves and Mean Flows* (monograph in preparation).

[76]N. H. Fletcher, R. K. Silk, and L. M. Douglas, "Acoustic admittance of air-driven reed generators," Acustica **50**, 155–159 (1982).

[77]J. C. Schelleng, "The violin as a circuit," J. Acoust. Soc. Am. **35**, 326–338 (1963); see also Erratum, J. Acoust. Soc. Am. **35**, 1291 (1963).

[78]Reference 1, Article 107.

[79]R. T. Schumacher, "Some aspects of the bow," Catgut Acoust. Soc. Newsletter **24**, 5–8 (1975).

[80]M. Hancock, "The mechanical impedances of violin strings," Catgut Acoust. Soc. Newsletter **23**, 17–26 (1975).

[81]G. Weinreich, "Coupled piano strings," J. Acoust. Soc. Am. **62**, 1474 (1977).

[82]C. Gough, "The resonant response of a violin G string and the excitation of the wolf note," Acustica **44**, 113–123 (1980).